The Company of **Biologists**

STEM CELLS AND REGENERATION

RESEARCH ARTICLE

The *miR-124* family of microRNAs is crucial for regeneration of the brain and visual system in the planarian *Schmidtea mediterranea*

Vidyanand Sasidharan[1,2,*], Srujan Marepally[1,*], Sarah A. Elliott[3,4], Srishti Baid[1], Vairavan Lakshmanan[1], Nishtha Nayyar[1], Dhiru Bansal[1,2], Alejandro Sánchez Alvarado[3,4], Praveen Kumar Vemula[1,‡] and Dasaradhi Palakodeti[1,‡]

ABSTRACT

Brain regeneration in planarians is mediated by precise spatiotemporal control of gene expression and is crucial for multiple aspects of neurogenesis. However, the mechanisms underpinning the gene regulation essential for brain regeneration are largely unknown. Here, we investigated the role of the *miR-124* family of microRNAs in planarian brain regeneration. The *miR-124* family (*miR-124*) is highly conserved in animals and regulates neurogenesis by facilitating neural differentiation, yet its role in neural wiring and brain organization is not known. We developed a novel method for delivering anti-miRs using liposomes for the functional knockdown of microRNAs. *Smed-miR-124* knockdown revealed a key role for these microRNAs in neuronal organization during planarian brain regeneration. Our results also demonstrated an essential role for *miR-124* in the generation of eye progenitors. Additionally, *miR-124* regulates *Smed-slit-1*, which encodes an axon guidance protein, either by targeting *slit-1* mRNA or, potentially, by modulating the canonical Notch pathway. Together, our results reveal a role for *miR-124* in regulating the regeneration of a functional brain and visual system.

KEY WORDS: Planarian, *Schmidtea mediterranea*, *miR-124*, Brain regeneration, Photoreceptors, Notch, miRNA

INTRODUCTION

Brain wiring is a complex process that ensures the formation of an intricate network of intercommunicating neurons. This process involves the precise guidance of axons from the neuron to its targets, which, in most animals, occurs during prenatal and early postnatal development (Tessier-Lavigne and Goodman, 1996; Stiles and Jernigan, 2010). Because of their unique capacity to regenerate a complex nervous system, planarian flatworms provide a suitable context in which to study factors essential for brain organization and neural patterning in adult animals. Planarians have a well-organized nervous system, which consists of a bi-lobed brain (cephalic ganglia) and a pair of ventral nerve cords interconnected by

commissural neurons (Umesono et al., 1999; Cebria et al., 2002a,b). The eyes are located dorsal to the cephalic ganglia. The planarian eye consists of pigment cells, which form a cup-shaped organ, and photosensing neurons that project rhabdomeres inside the pigment cup, while their axons form the optic chiasm (Sakai et al., 2000; Yamamoto and Agata, 2011). During planarian regeneration, the brain rudiment and eyes form within 24-48 h post-amputation (hpa). Although the differentiating primordia of the brain and eyes are evident ~3 days post-amputation (dpa), the recovery of the functional brain is completed only after 7 dpa (Inoue et al., 2004; Ong et al., 2016). Axon guidance proteins, such as those encoded by members of the *dscam*, *slit*, *netrin* and *robo* families, are essential for neural regeneration in planarians, and these factors are required for the patterning of the brain (Agata and Umesono, 2008; Yamamoto and Agata, 2011; Fusaoka et al., 2006; Cebria et al., 2007; Beane et al., 2012). However, the factors that regulate the spatiotemporal expression of these genes, which are crucial for the proper patterning of the planarian visual system and brain, are not known.

MicroRNAs (miRNAs) are small RNA species 21-22 nucleotides in length. They function in multiple biological processes, including neural stem cell proliferation, differentiation and patterning (Almuedo-Castillo et al., 2011; Plasterk, 2006; Hatfield et al., 2005; Thatcher and Patton, 2010). Deep sequencing of *Schmidtea mediterranea* small RNAs from the regenerating tissue (blastema) identified the *Smed-miR-124* family as the most prominent miRNAs enriched in the anterior blastema by 3 dpa (Sasidharan et al., 2013). The *miR-124* family is highly conserved across metazoa and is generally enriched in the nervous system (Kosik, 2009). Although the *miR-124* family is highly expressed in the adult brain of vertebrates, its role in adult neurogenesis is not known. Since whole-mount *in situ* hybridization (WISH) revealed that the *miR-124* family is enriched in the nervous system of the adult planarian (Gonzalez-Estevez et al., 2009; Sasidharan et al., 2013), we aimed to explore the function of this family, including its potential roles in neurogenesis.

We developed a novel liposome-based method for efficient delivery of *anti-miR-124* into live planarians to study the function of the *miR-124* family (hereafter collectively referred to as *miR-124*). Extensive characterization of *miR-124* knockdown (KD) phenotypes, which include severe brain and eye defects, revealed an essential role for *miR-124* in the generation and/or maintenance of discrete neural populations and eye progenitors, in addition to the patterning of neurons in the anteriorly regenerating planarian. Furthermore, *miR-124* KD caused an expansion of *Smed-slit-1* expression in the midline.

Target prediction analyses identified a cohort of genes essential for axon guidance, planar cell polarity, and the Notch pathway as likely targets of *miR-124*. To preliminarily validate our target predictions and gain insights into the mechanism of action of *miR-*

[1]Institute for Stem Cell Biology and Regenerative Medicine, GKVK campus, Bangalore, Karnataka 560065, India. [2]Manipal University, Manipal, Karnataka 576104, India. [3]Stowers Institute for Medical Research and Howard Hughes Medical Institute, Kansas City, MO 64110, USA. [4]Department of Neurobiology and Anatomy, University of Utah, Salt Lake City, UT 84112, USA.
*These authors contributed equally to this work

‡Authors for correspondence (praveenv@instem.res.in; dasaradhip@instem.res.in)

D.P., 0000-0003-2219-4785

DEVELOPMENT

124, we focused our efforts on the Notch pathway. The KD of Notch pathway genes recapitulated the midline defects observed after *miR-124* KD, suggesting that *miR-124* might regulate *slit-1* expression via the canonical Notch pathway. Altogether, our study uncovered roles for *miR-124* in neurogenesis and neuronal organization during adult brain and eye regeneration. Furthermore, we find that *miR-124* is likely to be required for midline patterning through a deeply evolutionarily conserved *miR-124/*Notch regulatory interaction.

RESULTS
Expression of the planarian *miR-124* family is enriched in the cephalic ganglia and ventral nerve cords

The planarian genome encodes five *miR-124* family members (*Smed-miR-124a*, *b*, *c*, *d* and *e*), which differ from each other after the tenth nucleotide from the 5′ end (Friedlander et al., 2009; Lu et al., 2009; Palakodeti et al., 2006). High-throughput sequencing of small RNAs from the anterior blastema of regenerating animals detected enrichment for *miR-124a*, *b*, *c* and *e* (Sasidharan et al., 2013). WISH using locked nucleic acid (LNA) detection probes

confirmed the expression of *miR-124a*, *b* and *c* in the cephalic ganglia and ventral nerve cords (Fig. S1A). The *miR-124e* detection probe was not used for further expression studies because of its weak and inconsistent staining. Colocalization of *miR-124a*, *b* and *c* with the pan-neural marker *Smed-pc2* and Hoechst staining revealed their expression in the bi-lobed cephalic ganglia. Unlike *miR-124a* and *b*, *miR-124c* showed a distinct expression pattern in the brain and ventral nerve cord, suggesting that the LNA probes effectively differentiate the expression of *miR-124c* from that of *miR-124a* and *b* (Fig. 1A,B, Fig. S1A-C). Additionally, *miR-124c* showed broad expression in both the perinuclear soma and the neuronal axon bundles in the bi-lobed cephalic ganglia, as compared with *miR-124a* and *b*, which were enriched in the perinuclear soma (Fig. 1B, Fig. S1B,C). Since *miR-124a* and *b* showed similar expression patterns, all additional expression studies were performed using the *miR-124b* probe. Colocalization studies of *miR-124b* and *miR-124c* with other neuronal markers, including *choline acetyltransferase* (*Smed-chat*), *glutamate decarboxylase* (*Smed-gad*), *tyrosine hydroxylase* (*Smed-th*) and *tryptophan hydroxylase* (*Smed-tph*),
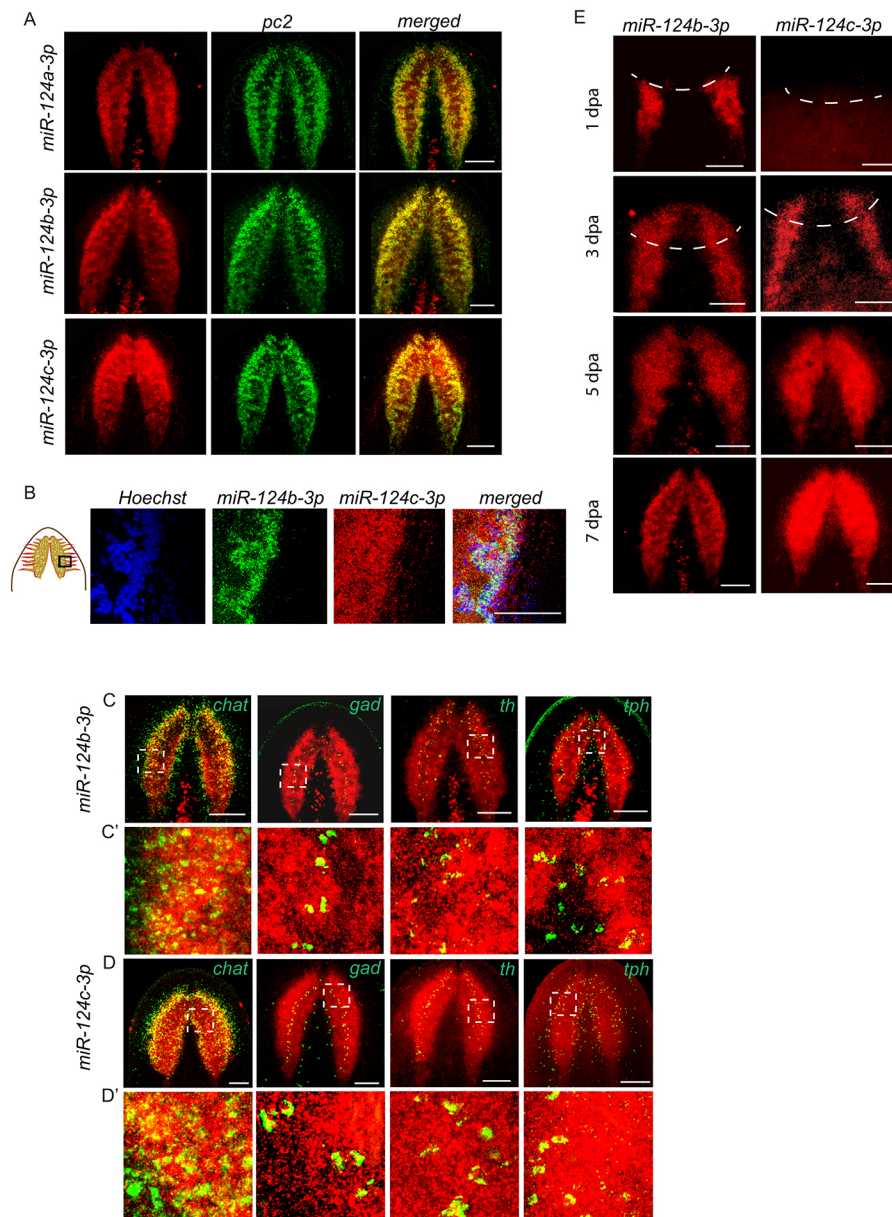

Fig. 1. Expression of *miR-124* family miRNAs in the planarian CNS. (A) Double fluorescent *in situ* hybridization (FISH) colocalization for *miR-124* family miRNAs with the pan-neuronal marker *pc2*. The merged images of double FISH show the expression of the miRNAs in the cephalic ganglia. (B) Differential expression of *miR-124* family miRNAs in the region indicated. (C-D′) *miR-124b* and *miR-124c* colocalize with different neuronal subtypes. (C,D) Double FISH was performed for *miR-124b* or *miR-124c* and cholinergic (*chat*), GABAergic (*gad*), dopaminergic (*th*) and serotonergic (*tph*) neuronal markers. (C′,D′) Higher magnification of the boxed regions from C and D. (E) *miR-124b* and *miR-124c* expression during regeneration. Dashed lines indicate the site of amputation. Scale bars: 100 μm.

revealed broad expression of *miR-124* in all of these neural subtypes (Fig. 1C,D, Fig. S2A,B).

Further examination of *miR-124b* and *miR-124c* expression at different regeneration time points (1, 3, 5 and 7 dpa) revealed their enrichment in the brain primordia as early as 3 dpa (Fig. 1E). Enrichment of *miR-124b* and *miR-124c* was also observed in the regenerating brain at 5 and 7 dpa, as well as in the anterior commissure that connects the bi-lobed structure (Fig. 1E). The expression of *miR-124c* in the pre-existing ventral nerve cords close to the regenerating brain was not seen until 3 dpa, whereas the expression of *miR-124b* was evident by 1 dpa (Fig. 1E). However, weak *miR-124c* expression was seen throughout the pre-existing ventral nerve cord between 3 and 7 dpa. Prominent expression of *miR-124c* throughout the ventral nerve cords was observed only after 7 dpa (Fig. S1D). Interestingly, the brain and eye primordia are known to begin forming between 1 and 2 dpa. Since none of the *miR-124* genes showed enrichment in the blastema until 3 dpa, this suggests that these miRNAs might contribute to the production of neural lineages born after 3 dpa and/or play roles in later stages of neural regeneration. To test these possibilities, we aimed to perturb the function of *miR-124* during planarian regeneration.

Design of non-viral liposomes for enhanced delivery of anti-miRs in planarians

Currently, the study of miRNAs in planarians is limited by the lack of effective methods for delivering anti-miRs into cells. Several methods, such as microinjection and soaking, have been used to deliver double-stranded RNA (dsRNA) into planarians (Orii et al., 2003; Sánchez Alvarado and Newmark, 1999; Martin-Duran et al., 2008; Gonzalez-Estevez et al., 2003). However, these methods have not proved to be successful for delivering anti-miRs (data not shown). To overcome this, we custom-designed cationic, non-viral liposomal vectors to deliver anti-miRs into planarian cells *in vivo*.

We designed cationic liposomes that are fluidic at lower temperatures (~25°C) to efficiently fuse with planarian cells. Cationic lipids with symmetric (di-octadecyl, Sym-Lip) and asymmetric (octadecyl and oleyl, Asym-Lip) hydrophobic chains were synthesized and characterized by mass spectrometry (Fig. 2A, Fig. S3A-F). The fluidity of liposomes was modulated by their preparation using a single lipid [either Sym-Lip (symmetric liposomes) or Asym-Lip (asymmetric liposomes)] or a 1:1 molar ratio of symmetric-asymmetric lipids (co-liposomes), along with cholesterol. The biophysical characterization of these three liposomes, including their size, surface charge and fluidity, revealed that co-liposomes are the best carriers of nucleic acids compared with symmetric and asymmetric liposomes (Fig. 2B,C). Furthermore, gel retardation studies of the three types of liposomes mixed with miRNAs at different concentrations revealed that all three liposomes efficiently complex with miRNA at a higher lipid-to-miRNA charge ratio of 20:1, inhibiting liposome mobility in the gel (Fig. 2D, Fig. S4A).

To evaluate the fusogenicity of cationic liposomes, we performed fluorescence resonance energy transfer (FRET) by reconstituting the liposome with planarian lipids (see Materials and Methods) using dual fluorophore lipids (NBD-PE and Rho-PE) (Fig. 2E). NBD-PE and Rho-PE in proximity have an emission wavelength of 595 nm due to FRET (Mukthavaram et al., 2009). Fusion of the liposome with the membrane leads to a spatial separation between NBD-PE and Rho-PE lipids, which results in emission at 530 nm instead of 595 nm owing to the absence of FRET. The total percentage of fluorescence recovery at 530 nm, as a direct measure of the fusogenicity of the liposomes (Fig. 2E,F), was 72%, 80% and

93% for the symmetric, asymmetric and co-liposomes, respectively. Additionally, no significant recovery (<5%) was observed for Lipofectamine RNAi Max (Thermo) (Fig. 2F). These data suggest that the cationic liposomes and co-liposomes were particularly efficient at inducing fusion with planarian lipid membranes when compared with Lipofectamine RNAi Max.

Transmission electron microscopy (TEM) was performed on the three liposomal formulations (Fig. 2G) and lipoplexes containing oligonucleotides. This demonstrated the unilamellar stable nature of the liposomes (Fig. S4B). Furthermore, fluorescently labeled oligonucleotide complexes with co-liposomes and Lipofectamine LTX were incubated with regenerating planarians, and confocal imaging revealed that co-liposomes have a better penetrance into tissues than Lipofectamine LTX (Thermo) (Fig. 2H, Fig. S5A). Confocal imaging of cell macerates from animals treated with co-liposomes further demonstrated that fluorescently labeled oligonucleotides successfully penetrate into the cytoplasm and nuclei of the cells (Fig. S5B). Cumulatively, these data indicate that these custom-designed liposomes could be highly efficient delivery vehicles for nucleic acids in planarians.

Knockdown of *ovo* and multiple miRNAs using non-viral liposomes

To validate the effectiveness of our liposome-based nucleic acid delivery method, we performed *ovo* KD. *ovo(RNAi)* animals are known to lack eyes. As expected, delivery of *ovo* dsRNA using liposomes resulted in an eyeless phenotype in 100% of the treated animals (*n*=15), whereas *gfp*-treated controls regenerated eyes normally (*n*=15) (Fig. 3A). This is on a par with the phenotype severity and penetrance obtained with dsRNA feeding or injection delivery methods (Lapan and Reddien, 2012).

Next, we examined the effectiveness of our delivery method for knocking down miRNAs. We administered an anti-miR that was predicted to target all *miR-124* family members using co-liposomes in regenerating animals at 1 dpa. Animals were treated with anti-miRs at 10, 50 and 100 μM, and a scrambled anti-miR negative control was used at 100 μM.

The miRNA KD was verified by examining expression of one of the *miR-124* family members, *miR-124c*, by WISH using antisense LNA probes. The animals treated with 50 or 100 μM anti-miRs showed significant decreases in expression of *miR-124c* (Fig. 3B). Although we observed a reduction in the expression of *miR-124c* in the 50 μM treatment condition, there was no obvious disorganization of the brain or visual system in these animals (Fig. S5C). This suggests that the reduction in *miR-124c* levels is not the result of a loss of brain tissue, but is specific to the inhibition of expression by the anti-miRs.

Since the anti-miRs are predicted to target all *miR-124* family members, we also examined the expression levels of another member of the family, *miR-124b*. As expected, we observed a significant decrease in *miR-124b* expression in the animals treated with 100 μM anti-miRs (Fig. S6A), suggesting that all *miR-124* members are likely to be inhibited. To assess whether the decreased levels of *miR-124* were due to reduction in brain size, we performed WISH for *miR-124a* and *miR-124c* on both control and KD animals after the first round of regeneration, when there were no observable defects in brain morphology (Fig. S6B). We detected a significant reduction in the levels of the two miRNAs, even though the cephalic ganglia were clearly present, suggesting that the reduction in miRNA levels is not the result of a smaller brain.

To confirm this, we performed qPCR for each *miR-124* family member after treatment with either the scrambled or anti-miRs.
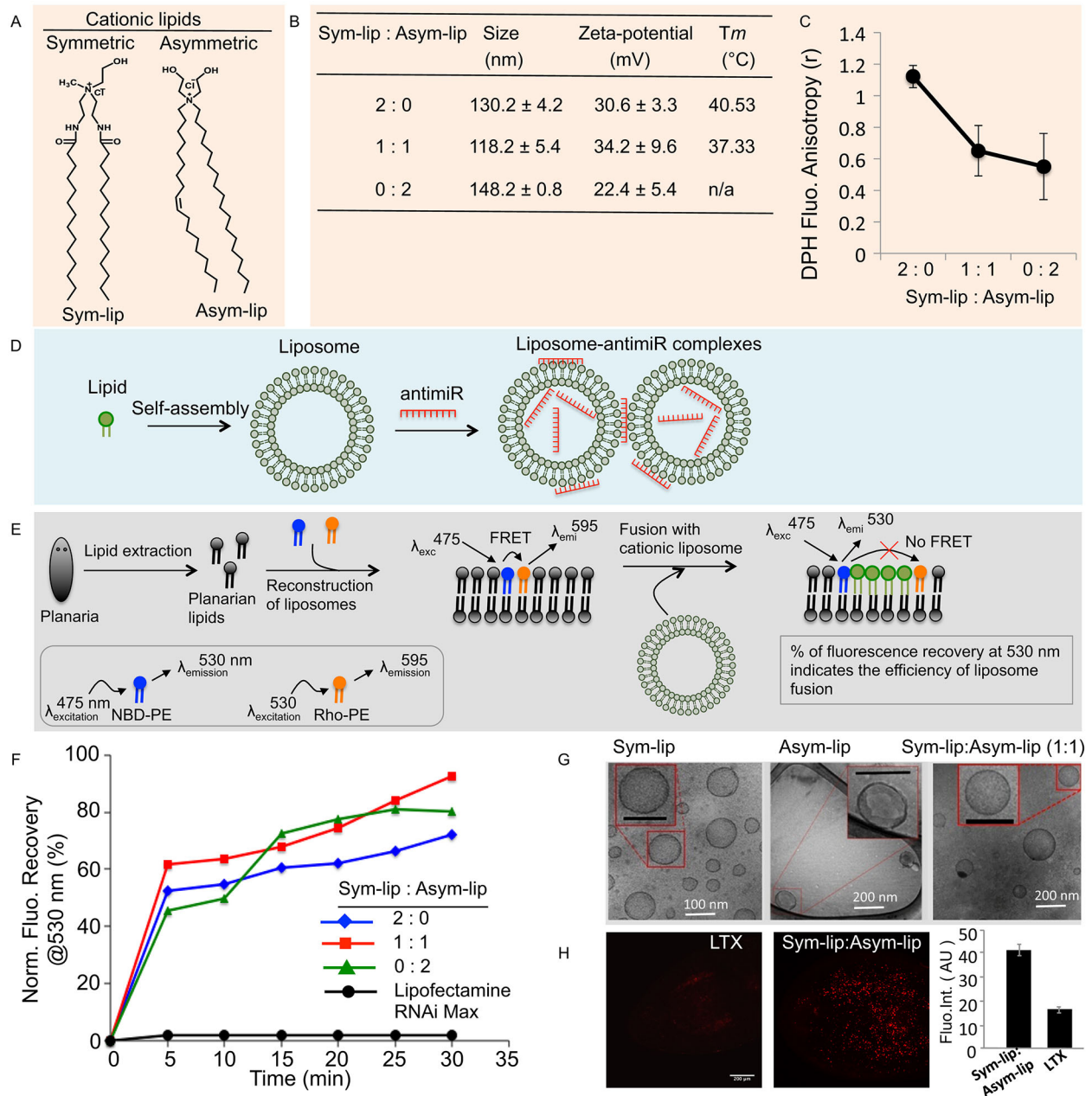
Fig. 2. Biophysical characterization of liposomes/lipoplexes and their fusogenicity with membranes. (A) Structures of symmetric and asymmetric cationic lipids. (B) Biophysical parameters of liposomes prepared using various ratios of lipids. (C) Fluorescence anisotropy measurement of diphenylhexatriene (DPH) in three types of liposomes, showing higher membrane fluidity of liposomes prepared using either asymmetric lipid or a 1:1 ratio of Sym-Lip and Asym-Lip. Error bars indicate s.d. (D) Schematic of lipoplex formation with anti-miRs and liposomes. (E) Scheme for reconstitution of the membrane using planarian lipids and fluorophore-tagged lipids (FRET pair of NBD-PE and Rho-PE). The proximity of the two fluorescent lipids in reconstituted planarian membrane enables FRET. Fusion of liposomes leads to separation of the fluorophores and inhibits FRET. Thus, emission of NBD-PE can be recovered. (F) Recovery of emission fluorescence at 530 nm indicates the higher fusogenic ability of cationic lipids over Lipofectamine. (G) TEM images of liposomes. (H) Confocal microscopy of planarians that were transfected with fluorescent dye-tagged anti-miRs using either the commercial agent Lipofectamine LTX or cationic liposomes. The bar chart shows the fluorescence intensity of Lipofectamine LTX and cationic liposomes (calculated using ImageJ). Error bars indicate s.d. Scale bar: 200 μm.

The anti-miR-treated animals showed a 50-90%, 30-40% and 20-40% decrease in the levels of *miR-124a*, *b* and *c*, respectively (Fig. S6C). This suggested that our liposome-based delivery method is robust.

Liposome-mediated miRNA KD generates highly penetrant and specific regeneration phenotypes

To determine whether the observed KD of miRNA expression translated into robust and specific regeneration defects in planarians,

we next examined the live phenotypes of planarians treated with *anti-miR-124*. Encouragingly, 81% of the animals treated with 100 μM anti-miRs showed various types of eye defects, including small eyes (25%), the complete absence of eyes (10%), cyclopia (13%), and eyes spaced abnormally far apart (14%) (Fig. 3C,D, Fig. S6D). A few animals (19%) also showed lesions in the head region and subsequently lysed (Fig. 3D).

To rule out the possibility that these regeneration defects might be due to unanticipated non-specific effects, we also treated planarians
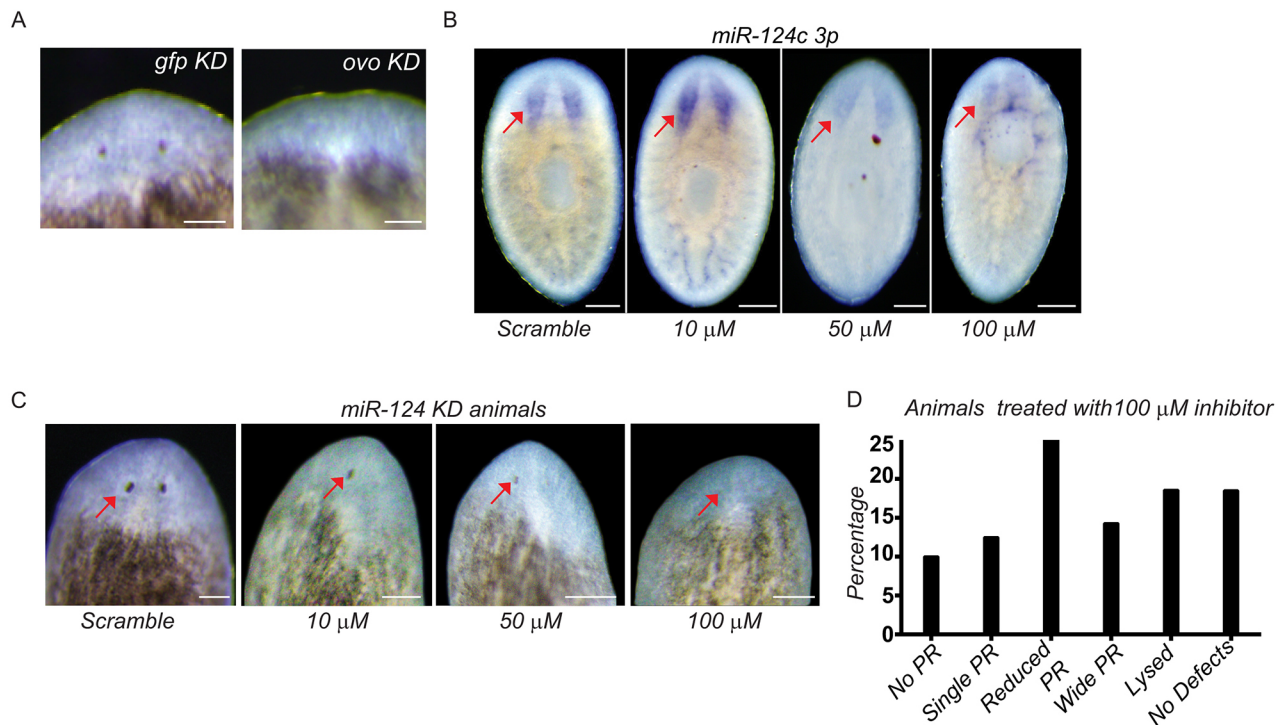
DEVELOPMENT

Fig. 3. Validation of liposome-mediated *ovo* and *miR-124* KD. (A) *ovo(RNAi)* animals (15/15) showed an eyeless regeneration phenotype in the first round of anterior regeneration after 7 dpa. (B) WISH showing the expression of *miR-124c* at 7 dpa during the second round of regeneration in KD animals (*n*=5). (C) Animals treated with 100 μM scrambled miRs rarely showed regeneration defects (4/90, 4.4%), whereas 10 μM (7/33, 21.2%), 50 μM (12/33, 36%) or 100 μM (91/112, 81%) anti-miR-treated animals frequently showed eye regeneration defects. Arrows indicate eye in the scrambled-treated or anti-miR-treated animals. Scale bars: 100 μm. (D) The percentage of animals that show various categories of photoreceptor (PR) defects observed in regenerated animals following 100 μM anti-miR treatment.

with anti-miRs targeting the *miR-10* family. We observed a phenotype entirely different from that of *miR-124* KD animals. No defects in the regeneration of the eyes or brain were observed. Instead, the regeneration of the intestine was disrupted, resulting in fusion of the two posterior gut branches (Fig. S6E,F).

Cumulatively, these validation experiments indicate that our liposome-based technique is highly specific and robust for delivering anti-miRs into planarian cells for functional studies.

miR-124 is essential for regeneration of the eye in planarians

Since we observed obvious eye defects in live animals, we examined the morphology of the regenerated optic cup in *miR-124* KD animals. Using an anti-ARRESTIN antibody that labels the cell bodies, rhabdomeres and axons of the photoreceptor neurons (PRNs), we observed that *miR-124* KD animals displayed obvious fasciculation and elongation defects of the axons. The optic chiasm appeared highly disorganized (Fig. 4A,B). Furthermore, the aggregation of PRN cell bodies appeared significantly reduced in *miR-124* KD animals compared with scrambled controls (Fig. 4A, arrowheads), suggesting that this differentiated cell population might be missing after loss of *miR-124*.

Since we suspected that the numbers of differentiated cells of the eye were decreased in *miR-124* KD animals, we quantified the size of the regenerated eyes. We performed FISH for *ovo*, which labels the entire eye lineage, including the terminally differentiated cells of the pigment cup and PRNs (Lapan and Reddien, 2012). The size of the eyes was quantitated by measuring the area of *ovo* staining in the differentiated eye normalized to the total body area or brain size (Fig. 4C, Fig. S7A). As expected, *miR-124* KD animals showed a significant decrease in the overall size of the regenerated eyes

compared with scrambled-treated controls, suggesting a reduction in the number of differentiated cells. To confirm this, we counted individual ARRESTIN[+] PRNs in the regenerated eyes. There were significantly fewer ARRESTIN^{+} cells in *miR-124* KD animals than in the scrambled-treated controls, confirming that this cell population was lost (Fig. S7B).

A reduction in the number of differentiated cells could mean that eye progenitors are lost after KD of *miR-124*. Therefore, we quantified the number of eye progenitors at 4 dpa, which are defined as *ovo*[+] 'trail' cells posterior to the eye primordia (Lapan and Reddien, 2012). Indeed, the number of *ovo*^{+} trail cells was significantly reduced in *miR-124* KD animals (Fig. 4D), suggesting that *miR-124* may be required for the specification, differentiation and/or survival of eye progenitors.

miR-124 is required for regeneration of the cephalic ganglia

Since *miR-124* family members are highly enriched in the nervous system, we examined whether brain regeneration was affected by loss of these miRNAs. Indeed, some *miR-124* KD animals (16%) displayed a reduction in the overall size of the brain compared with scrambled-treated controls, which was evident by immunostaining for the broad neural marker SYNORF-1 (Fig. 4E,F).

The planarian brain is composed of different neuronal subtypes (Roberts-Galbraith et al., 2016; Cowles et al., 2013; Ong et al., 2016). To explore the neural defects, we examined three of the major neuronal subtypes in planarians after *miR-124* KD: the dopaminergic (*th*[+]), GABAergic (*gad*[+]) and cholinergic (*chat*^{+}) neurons. FISH revealed a dramatic decrease in the numbers of *gad*[+] and *th*^{+} cells in *miR-124* KD animals compared with scrambled-
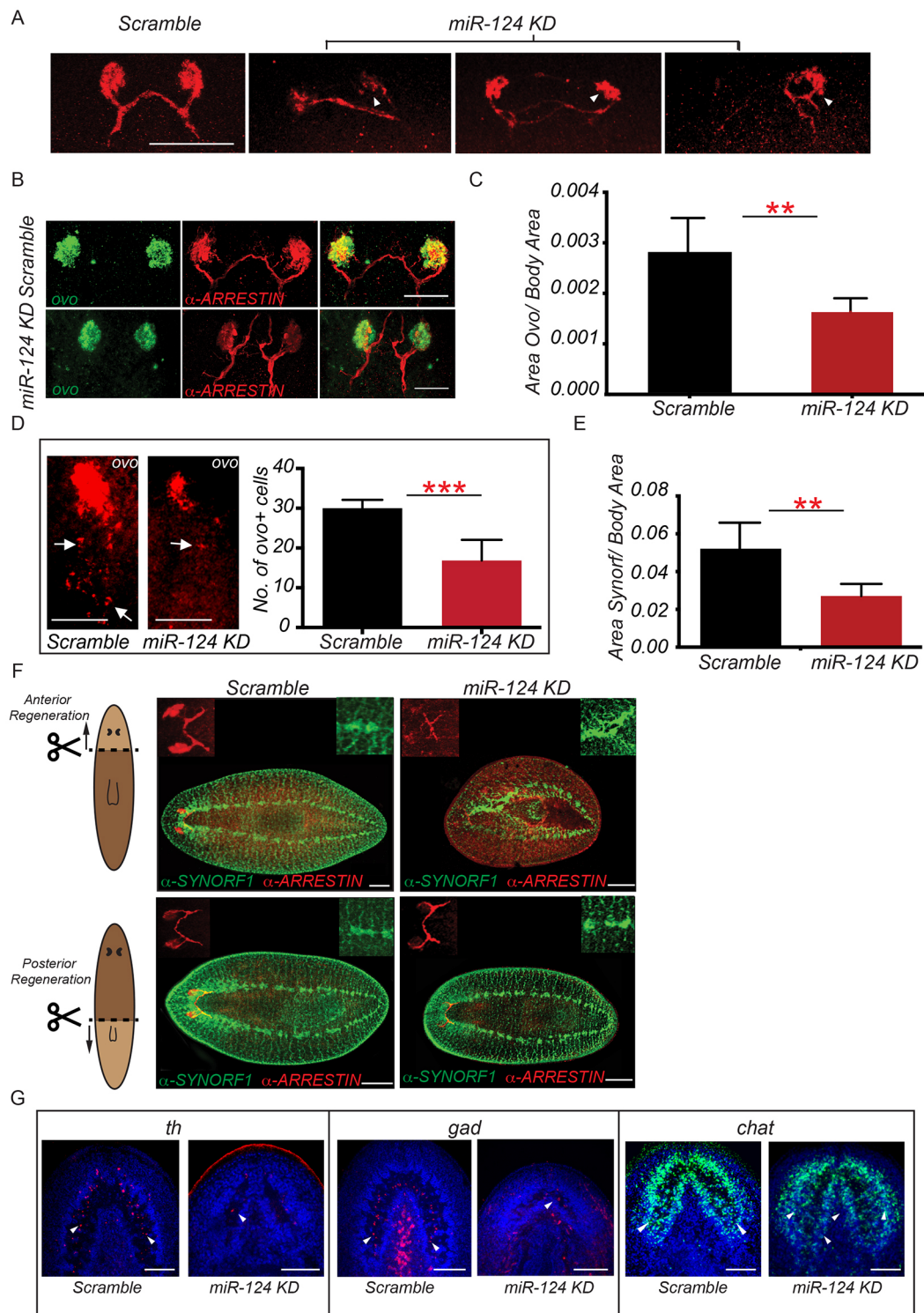
Fig. 4. See next page for legend.

treated controls, suggesting a loss of GABAergic and dopaminergic neurons. Interestingly, KD of *miR-124* caused a significant increase in the number of *chat*+ cells, indicating a likely expansion of cholinergic neurons (Fig. 4G, Fig. S7C).

Since a disruption in differentiated neural cell types and a reduction in the size of the brain might indicate defects in the generation and/or maintenance of neural progenitors, we examined the expression of a progenitor marker for the nervous system (*Smed-pax6A*) (Wenemoser

et al., 2012). In *miR-124* KD animals, no reduction in the expression of *pax6A* was observed at 4 dpa (Fig. S7D). However, the KD animals showed mispatterned expression of *pax6A*+ cells. This suggested that *miR-124* might not be required for the initial generation of neural progenitors, but may instead be required later during the progression of the lineage. Cumulatively, these data indicate that *miR-124* may be involved in the production of discrete neural subpopulations during planarian brain regeneration.

Fig. 4. *miR-124* KD disrupts regeneration of the eyes and brain.
(A) Immunostaining of the optic chiasm (anti-ARRESTIN) in scrambled-treated versus anti-*miR-124*-treated animals (100 µM each) at 7 dpa after the second round of regeneration. 13/16 KD animals showed diverse eye defects. Arrowheads indicate defects in KD animals. (B) FISH showing the expression of *ovo* in the eye and immunostaining for photosensory neurons (anti-ARRESTIN) in *miR-124* KD (*n*=10) and scrambled-treated (*n*=7) animals. (C) Quantification of the size of the eyes determined by the ratio of the area of *ovo* staining to the total body area in scrambled-treated (*n*=6) versus anti-*miR-124*-treated (*n*=5) animals. (D) FISH showing the expression of *ovo* in the eye and trail cells posterior to the eye in scrambled-treated and *miR-124* KD animals at 4 dpa (*n*=6 animals per treatment condition). *ovo*⁺ trail cells were quantified in each condition. (E) Quantification of anti-SYNORF-1 staining of anteriorly regenerating animals normalized to body area in scrambled-treated versus anti-*miR-124*-treated (100 µM) animals (*n*=5 each). (F) Organization of the brain, ventral nerve cords, (anti-SYNORF-1, green) and photosensory neurons (anti-ARRESTIN, red) in scrambled (10/10) versus *miR-124* KD animals regenerating either a head (10/10; top) or tail (13/16; bottom). Illustrations show the amputation plane (dashed line) and lighter colored areas indicate regenerated tissue. (G) FISH for neuronal subtypes in the brain of scrambled-treated versus *miR-124* KD animals, including dopaminergic (*th*, red; *n*=6), GABAergic (*gad*, red; *n*=6) and cholinergic neurons (*chat*, green; *n*=6). Nuclei are stained with Hoechst (blue). Arrowheads indicate the neural subtypes. **P<0.01, ***P<0.001 (Student's *t*-test). Error bars indicate s.d. Scale bars: 50 µm in A,B,D; 100 µm in F,G.

We also tested whether *miR-124* is required in regeneration contexts that do not involve rebuilding organs from scratch. First, we examined the head fragments that only regenerate tissues posterior to the brain *de novo*. In these animals, the pre-existing brain and eyes undergo remodeling and resizing, which is dependent on tissue turnover (Gurley et al., 2010). *miR-124* KD animals regenerating posterior tissue showed no defects in the brain, eyes or optic chiasm, suggesting that *miR-124* is not required for brain remodeling in posteriorly regenerating animals (Fig. 4F).

We also examined these organs during homeostatic tissue turnover after *miR-124* KD. Intact animals were continuously treated with anti-miR for 1 month. No defects in the organization of the nervous system or eyes were observed after *miR-124* KD

compared with scrambled-treated controls (Fig. S7E). These results suggest that *miR-124* is primarily required during *de novo* regeneration of the cephalic ganglia, ventral nerve cords and visual system in planarians.

miR-124 eye regeneration defects are independent of brain defects

Brain malformations are known to cause secondary defects in the eyes of planarians (Cowles et al., 2013). Therefore, it is possible that the observed eye defects upon *miR-124* KD might be secondary to abnormalities present in the brain. To help address this, we examined the function of *miR-124* during eye-only regeneration in the absence of any brain defects. This was achieved by first generating *ovo(RNAi)* worms, which lacked eyes but did not display brain abnormalities or any other morphological defects (Lapan and Reddien, 2012) (Fig. 5A,B). Next, we stopped the treatment with *ovo* dsRNA, which allowed the eyes to progressively regenerate over the course of 1 month as the gene expression recovered. During this recovery period, we treated animals with either scrambled or anti-*miR-124*, and assessed whether the eyes could regenerate in the presence of otherwise normal anatomy (Fig. 5A,B). The scrambled-treated live animals clearly regenerated eyes, whereas the animals treated with anti-*miR-124* showed no signs of eye recovery at the same time point (Fig. 5C). To confirm this, we visualized the differentiated PRNs (*Smed-opsin*), optic chiasm (anti-ARRESTIN) and pigment cells (*Smed-tyrosinase*) in fixed worms. Consistent with our live animal observations, scrambled-treated worms regenerated both PRNs and pigment cells, in addition to a well-organized optic chiasm. By contrast, *miR-124* KD animals possessed significantly fewer mature pigment cup cells and PRNs. Additionally, the axons projected by the few PRNs that were present after *miR-124* KD did form an optic chiasm, but mistargeting of some axons was observed (Fig. 5D). Cumulatively, the results of this eye-specific regeneration paradigm suggest that *miR-124* has a direct role in eye regeneration, and this eye phenotype is unlikely to be a secondary effect of a generalized brain defect.
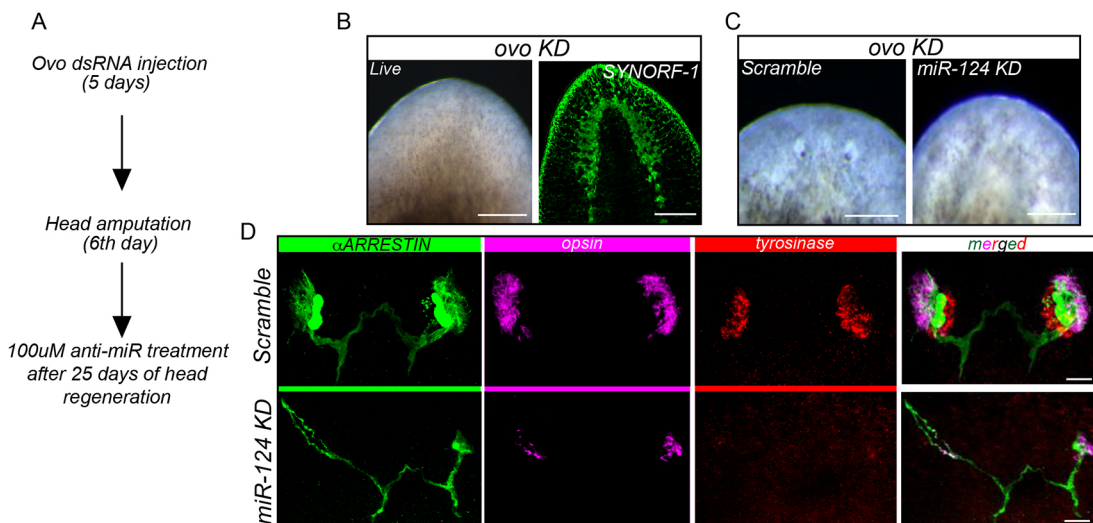

Fig. 5. *miR-124* is required for eye-specific regeneration. (A) Methodology of eye-specific regeneration experiments. *ovo* dsRNA was administered by injection for 5 days, and on the sixth day the animals were amputated pre-pharyngeally. LNA anti-miRs were administered on alternative days for 8 days after 25 days of head regeneration. (B) Live images and anti-SYNORF-1 staining of *ovo* KD animals after 25 days of RNAi (*n*=15 animals). (C) Live images of *ovo* KD animals showing recovery of eyes after scrambled treatment (*n*=15/15 recovery) but not after anti-*miR-124* treatment (*n*=12/15 failure). (D) Molecular characterization of eye phenotypes using anti-ARRESTIN (photosensory neurons and axons), opsin (photosensory neuron cell bodies) and *tyrosinase* (pigment cup cells). *miR-124* KD animals (10/12) showed drastic reduction in *opsin* and *tyrosinase* staining, along with mispatterned photoreceptor neurons. Scale bars: 100 µm in B; 50 µm in C,D.

The putative targets of *miR-124* are crucial for neuronal organization and growth

In an effort to identify the transcripts regulated by *miR-124*, we performed target prediction using the miRanda program (Enright et al., 2003). Target prediction identified a total of 1699 putative targets that might be regulated by the *miR-124* family (Table S1). Although most of the predicted targets were common between all the *miR-124* family miRNAs, we identified 128 and 125 predicted targets unique to *miR-124b* and *miR-124c*, respectively. Gene set enrichment analysis (GSEA) (Subramaniam et al., 2005; Mootha et al., 2003) of *miR-124* targets identified genes normally involved in axon guidance (*slit-1*, *dscam*, *netrin-1*), Notch signaling (*notch-2*, *jagged-2*) and planar cell polarity (PCP) (*dishevelled-2*, *daam-1*) (Table S2, Fig. S8A). Most have been shown to regulate visual neuronal organization and neuronal growth in planarians (Yamamoto and Agata, 2011; Fusaoka et al., 2006; Cebria et al., 2007; Gurley et al., 2008; Almuedo-Castillo et al., 2011; Beane et al., 2012).

We validated some of the predicted targets of *miR-124*, including *dscam*, *slit-1*, *ankyrin-3* and *notch-2*, by cloning their miRNA binding sites into the 3′-UTR region of the Firefly luciferase gene, followed by transfection into HEK293 cells. Upon *miR-124* mimic transfection, we observed a 24-50% decrease (*notch-2*, 24%; *dscam*, 37%; *slit-1*, 50%; *ankyrin-3*, 43%; $P<0.05$) in Firefly luciferase activity compared with controls (Fig. 6A, Fig. S8B). These results show that the tested 3′-UTRs are likely targets of *miR-124 in vivo*.

Furthermore, we performed transcriptome sequencing to determine the transcriptional changes following *miR-124* KD. The transcriptome sequencing identified 2609 transcripts that were differentially expressed ($P<0.05$). Of these, 1523 were significantly upregulated (Table S3). We used qPCR to examine the expression levels of 30 of these transcripts, and validated 25 that were significantly upregulated after *miR-124* KD ($P<0.05$; Fig. S8C). The other five were upregulated by more than 2-fold, showing a similar trend to the transcriptome data, although not statistically significant. Among the 25 validated transcripts, nine were predicted as targets by miRanda. Interestingly, our data also show that most of the miRanda predicted targets were either marginally upregulated or show no change in expression upon *miR-124* KD. It has previously been reported that *miR-124* could potentially function by repressing mRNA translation rather than promoting transcript degradation (Hendrickson et al., 2009). Here we hypothesize that most of the targets of *miR-124* that are only marginally upregulated upon *miR-124* KD might be regulated by translational repression.

Mediolateral polarity is disrupted by loss of *miR-124*

The disruption of anteroposterior (A/P) or mediolateral (M/L) polarity might cause the observed eye and brain defects in *miR-124* KD animals (Gurley et al., 2008). To determine whether the *miR-124* KD phenotype is secondary to a polarity defect, we first investigated the organization of an organ system that is often disrupted by perturbation of these axes: the intestine (*Smed-porcn-1⁺*) (Rink et al., 2009; Petersen and Reddien, 2009; Gurley et al., 2010; Cebria et al., 2007). We found that the intestines were indistinguishable between *miR-124* KD animals and controls (Fig. 6B). No fusion of the posterior gut branches, ectopic or missing pharyngeal cavities, or additional major gut branches were observed, which are typical defects in worms with generalized A/P or M/L disruption.

We next examined whether A/P and M/L markers were likely to be targets of *miR-124*. Furthermore, we performed WISH to check
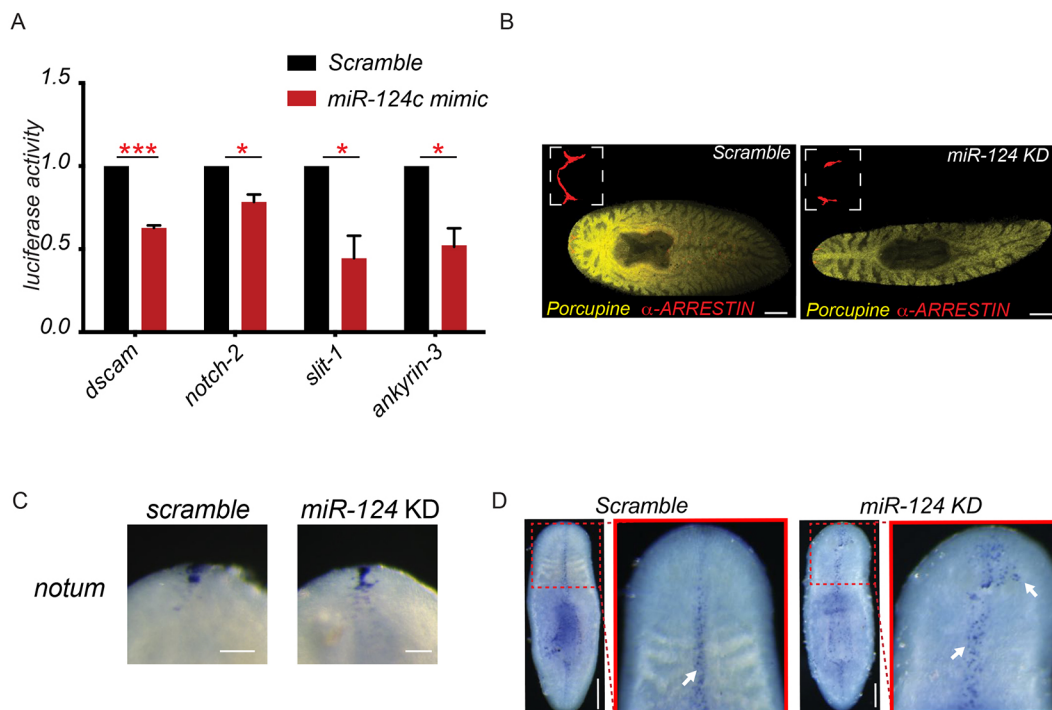

Fig. 6. Target prediction to identify *miR-124* targets. (A) Luciferase assay was carried out to validate miRNA targets. *$P<0.05$, ***$P<0.001$ (Student's *t*-test). Error bars indicate s.d. (B) FISH for *porcupine-1* revealed that the organization of the intestine is indistinguishable between scrambled-treated and anti-*miR-124*-treated animals. (C) WISH for *notum* in scrambled-treated and anti-*miR-124*-treated animals (D) Colorimetric WISH showing *slit-1* expression in scrambled-treated and anti-*miR-124*-treated animals at 7 dpa from the second round of regeneration. Arrows indicate the expression of *slit-1* in the midline region. Scale bars: 100 μm.

for the expression of *Smed-notum*, an anterior marker and key regulator of A/P polarity (Petersen and Reddien, 2011), at 2 dpa in scrambled-treated versus *anti-miR-124*-treated animals (Fig. 6C). No difference in *notum* expression was observed between the control and KD animals. Cumulatively, this suggests that A/P polarity is not disrupted by *miR-124* KD.

By contrast, *slit-1*, a broad marker for the midline, was a predicted target of *miR-124*. WISH for *slit-1* revealed the presence of ectopic *slit-1*^{+} cells in the anterior blastema after KD of *miR-124* (Fig. 6D). Interestingly, the loss of *slit-1*, not its expansion, is typically associated with a reduction in brain size and cyclopia (Cebria et al., 2007) like that we observe after *miR-124* KD. These data suggest that the eye and nervous system abnormalities in *miR-124* KD animals are unlikely to be secondary to a generalized loss of A/P or M/L polarity.

miR-124 may regulate the *slit-1*-expressing midline via canonical Notch signaling

Finally, we aimed to provide functional evidence that this list of predicted *miR-124* targets can yield insights into the undoubtedly complex functions of this miRNA family during planarian regeneration. As a pilot experiment, we selected *notch-2* as a candidate for functional analysis because a previous RNAi screen in the lab indicated that canonical Notch signaling might be involved in regulation of the midline, which we knew to be disrupted after *miR-124* KD.

Knockdown of *notch-2*, which is broadly expressed throughout the planarian body (Fig. 7A), resulted in conspicuous regeneration defects that are typically associated with disruption of the midline. Specifically, *notch-2(RNAi)* animals displayed cyclopia and fusion of the two posterior gut branches (Fig. 7B,C). Since these defects are similar to those reported after RNAi of *slit-1* (Cebria et al., 2007), we examined the expression of *slit-1* after RNAi of *notch-2*. As expected, *notch-2(RNAi)* animals displayed a significant reduction in the number of *slit-1*^{+} cells (Fig. 7D). Interestingly, RNAi of other components of the canonical Notch pathway, including the core transcription factor *Su(H)* and the ligand *delta-3*, resulted in very similar midline defects. These included cyclopia, fusion of the posterior gut branches, and loss of *slit-1* expression (Fig. S9A-J). Furthermore, RNAi of a negative regulator of Notch signaling, *numb-1*, yielded the opposite phenotype: a conspicuous increase in *slit-1*^{+} cells (Fig. 7E,F), which appeared strikingly similar to the phenotype observed for *slit-1* expression after *miR-124* KD.

Next, we investigated whether the effects on *slit-1* expression are likely to be direct effects of *notch-2/miR-124* regulation. We first examined colocalization of the *notch-2* receptor and the *delta-3* ligand in the *slit-1*[+] population. This revealed that *notch-2* and *delta-3* are both expressed in discrete subpopulations of *slit-1*^{+} cells and in cells directly adjacent to *slit-1*^{+} cells (Fig. S10). Since Notch/Delta signaling is cell-autonomous, this suggests the possibility of a direct role for Notch signaling in regulating the *slit-1*-expressing midline.
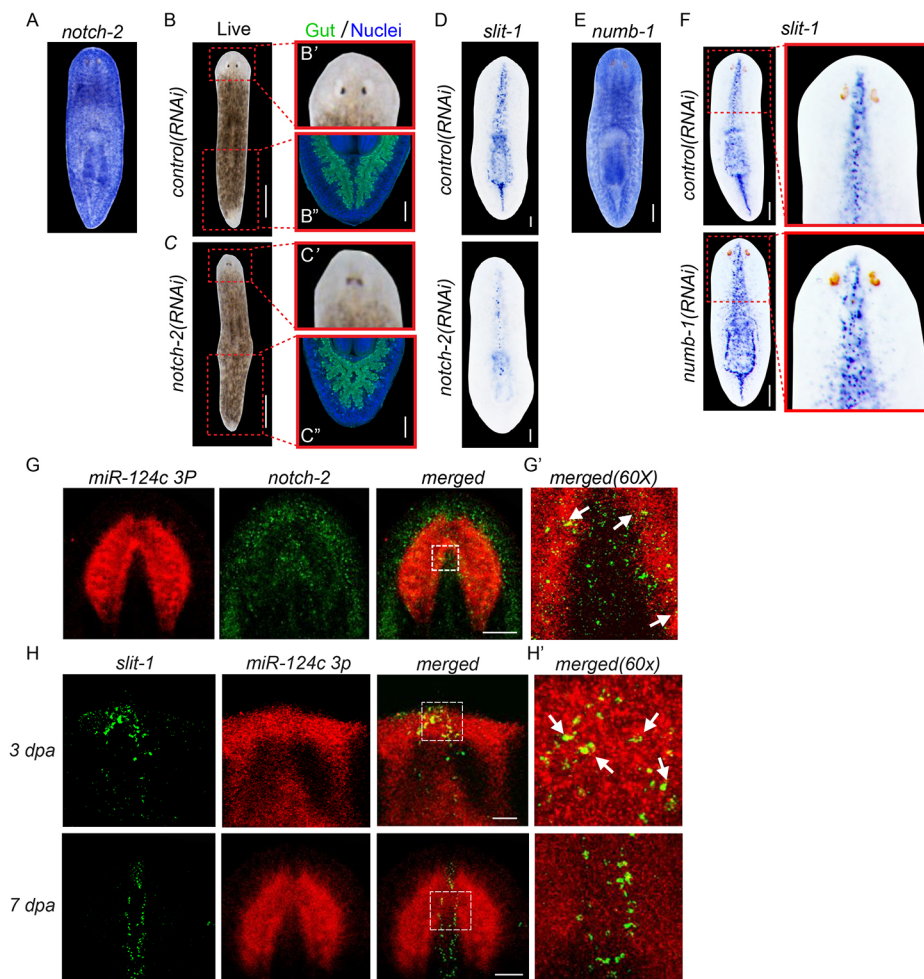

Fig. 7. Regulation of *notch-2* and *slit-1* by *miR-124*. (A) Colorimetric WISH shows broad expression of *notch-2* in uninjured planarian. (B-C″) *notch-2* KD leads to cyclopia (B′ versus C′; 14 dpa) and fusion of posterior gut branches (B″ versus C″; *mat*, green; DAPI, blue; 17 dpa). (D) Colorimetric WISH for *slit-1* after long-term *notch-2* RNAi. *slit-1* is significantly reduced in *notch-2(RNAi)* planarians compared with controls. (E) Colorimetric WISH shows broad expression of *numb-1* in uninjured planarian. (F) Colorimetric WISH for *slit-1* in control versus *numb-1(RNAi)* planarians at 23 dpa. Higher magnification images of the head show ectopic *slit-1*^{+} cells in *numb-1(RNAi)* planarians. (G,G′) Double FISH showing colocalization (arrows) of *miR-124c* (red) and *notch-2* (green). (H,H′) Double FISH for *slit-1* and *miR-124c* during anterior regeneration. *miR-124c* colocalizes with *slit-1* (arrows) at 3 dpa, but not at 7 dpa. Scale bars: 100 μm.

We also examined the expression of *miR-124* in both *notch-2*[+] and *slit-1*^{+} cells. We found co-expression of *notch-2* and *miR-124c* in the periphery of the brain in uninjured animals (Fig. 7G,G'). During head regeneration, a subset of *miR-124*^{+} cells colocalized with *slit-1* at 3 dpa, but not at 7 dpa (Fig. 7H,H', Fig. S9K). These expression dynamics suggest that *miR-124* has the potential to function cell-autonomously in *notch-2*[+] and *slit-1*^{+} cells.

Cumulatively, these phenotype and expression data suggest that the expansion of the *slit-1*-expressing cell population observed after *miR-124* KD may be mediated via direct regulation of *notch-2* and subsequent canonical Notch signaling in planarians. Moreover, this indicates that our list of predicted targets of *miR-124* promises to be extremely useful for further dissecting the complex roles of this miRNA family in the regeneration of the brain, visual system and midline of planarians.

DISCUSSION

Although several genes crucial for anterior fate determination and nervous system regeneration have been identified (Vasquez-Doorman and Petersen, 2014; Fraguas et al., 2014; Blassberg et al., 2013; Roberts-Galbraith and Newmark, 2013; Agata and Umesono, 2008; Beane et al., 2011; Higuchi et al., 2008; Gurley et al., 2008; Rink et al., 2009; Bonar and Petersen, 2017; Seebeck et al., 2017; Currie et al., 2016; Wang et al., 2016; Roberts-Galbraith et al., 2016; Adell et al., 2010), how these genes are coordinated in time and space to establish the developmental transitions necessary for form and function of the nervous system remains to be fully elucidated. Our study has revealed enrichment for the *miR-124* family of miRNAs in the nervous system of planarians during homeostasis and discrete phases of head regeneration. The expression of *miR-124c* and *miR-124b* observed in anteriorly regenerating tissue at 3 dpa (Fig. 1E) suggests that these miRNAs might play a role in the organization of the brain and the patterning of visual neurons, rather than in specification of the brain primordium. We tested this hypothesis by perturbing the function of *miR-124* during planarian regeneration.

To perform loss-of-function studies for *miR-124* in planarians, we developed a novel vehicle to deliver anti-miRs using co-liposomes (Fig. 2). This method proved superior to soaking and injection, and we observed a comparably higher success rate for miRNA-mediated and also dsRNA-mediated KD using co-liposomes (Fig. 3, Fig. S5). *miR-124* KD animals regenerating anterior tissue had either reduced or absent photoreceptors. Interestingly, the posterior regenerating tissue and the intact animals did not show any regeneration defects. However, the lack of homeostatic defects in *anti-miR-124* KD animals might simply reflect slow turnover rates for neural cell types and/or the targeted mRNAs and proteins.

Extensive characterization of *miR-124* KD planarians using various brain- and eye-specific markers revealed diverse defects in the organization of the brain and visual neurons. The diverse phenotypes observed might be attributed to variability in the extent of KD or to changes in the large cohort of genes with varied functions in *miR-124* KD animals. Our study also revealed the key role of *miR-124* in regulating neural subtype specificity and organization during planarian regeneration. For instance, *miR-124* KD led to a reduction in the number of GABAergic and dopaminergic neurons, in addition to an increase in cholinergic neurons. However, the pathway through which *miR-124* regulates neural subtype specificity is not known. Nonetheless, our data provide robust evidence for an important role for *miR-124* in brain organization, the generation and/or maintenance of eye progenitors, and visual system patterning in regenerating planarians (Fig. 8A). Furthermore, our work also highlights the need to invest time and effort in developing novel liposome vehicles, which might help advance the development of transgenic methods in planarians.

Target prediction revealed a cohort of genes involved in PCP (*disheveled-2*, *daam-1*), axon guidance (*netrin-1*, *slit-1*, *dscam*) and the Notch pathway (*notch-2*, *delta-3*, *serrate-1*) as predicted targets of *miR-124*. Interestingly, *miR-124* target conservation across the metazoans revealed that some of the planarian *miR-124* targets, particularly *notch-2*, *netrin-1* and *slit-1*, are also targets of *miR-124* in vertebrates, but not in flies and nematodes (Fig. S11, Table S4). This is a notable difference given the extensive functional conservation in neurogenesis ascribed to *miR-124* (Cao et al., 2006, 2007). There might be several biological and
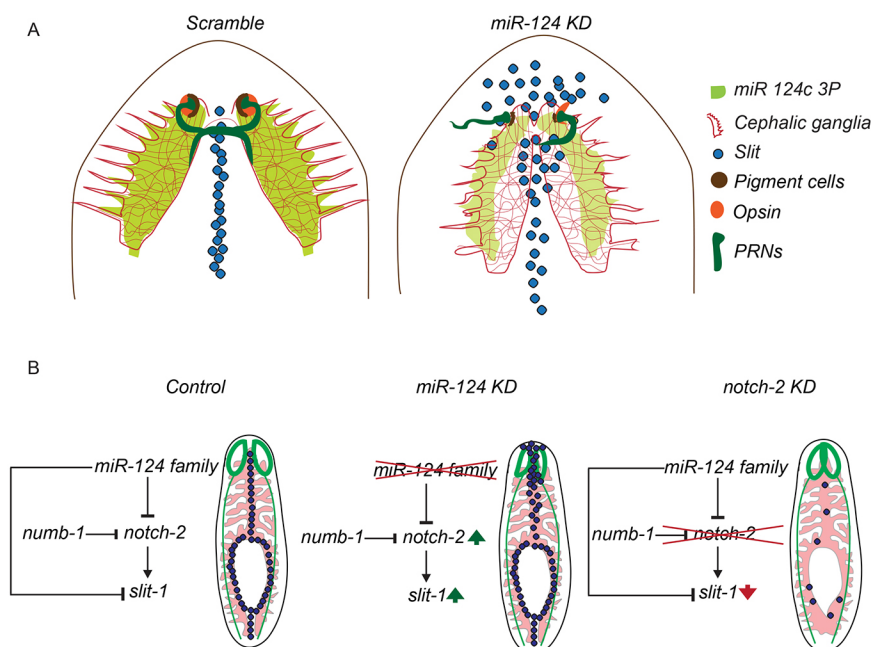

Fig. 8. Summary of *miR-124* function during planarian regeneration. (A) Schematic of the brain, eye and midline after head regeneration in *miR-124* KD versus control planarians. KD of *miR-124* causes a reduction in the size of the cephalic ganglia, a loss of eye cells, disorganization of the optic chiasm, and an expansion of the *slit-1*[+] midline population. (B) Proposed genetic interaction in which *miR-124* modulates *slit-1* via inhibition of *notch-2* expression. The schematic also summarizes the organization of the regenerated brain (green), gut (pink) and *slit-1*[+] midline (black) following KD of *miR-124* or *notch-2*.

methodological reasons for this difference. First, it might be that only vertebrates have evolved the ability for *miR-124* to target *notch*, *netrin* and *slit* orthologs, and that the target predictions obtained for planarians might be an artifact. The evolutionary argument seems unlikely given that, in the invertebrate *Ciona intestinalis*, a feedback interaction between *miR-124* and Notch signaling regulates the epidermal-peripheral nervous system (PNS) fate choice in tail midline cells (Chen et al., 2011). These findings suggest that our target predictions are not only biologically relevant, but also that they point to an ancestral origin of the regulation of the Notch pathway by the *miR-124* family of miRNAs. Such a regulatory nexus might have been lost in *C. elegans* and *D. melanogaster*.

Among the putative *miR-124* targets, three genes encoding axon guidance proteins were uncovered. *netrin-1* and *dscam* are expressed in the planarian brain, while *slit-1* is expressed in the midline along the length of the A/P axis of planarians (Yamamoto and Agata, 2011; Fusaoka et al., 2006; Cebria et al., 2007). The spatial and temporal expression of these genes is essential for proper patterning of the brain and the visual neurons. For instance, perturbation of *slit-1* expression in the midline resulted in the collapse of the photoreceptors, demonstrating the key role for *slit-1* in proper patterning of the visual neurons to form the optic chiasm. Furthermore, our expression study based on double FISH for *slit-1* and *miR-124* in regenerating animals revealed spatial and temporal changes in the expression of these genes in the midline region of anteriorly regenerating tissue. Thus, we hypothesize from these data that *miR-124* expression in the brain might be essential for regulation of *slit-1* expression during anterior regeneration. This hypothesis was supported by the *miR-124* KD studies, which showed increased levels of *slit-1* expression in the anterior region of the regenerating planarian. However, the expression of *miR-124* is neuronal, except at 3 dpa when *miR-124* was seen in *slit-1*⁺ cells, whereas the expression of *slit-1* is non-neuronal. This raises an important question regarding the molecular mechanism by which *miR-124* regulates the expression of *slit-1*. Our study has demonstrated that KD of *notch-2* and *delta-3* led to downregulation of *slit-1*, and KD of its negative regulator *numb-1* caused ectopic expression of *slit-1*. The *notch/numb* KD studies were supported by colocalization studies, which showed co-expression of *delta-3* and *notch-2* in *slit-1*⁺ cells, suggesting that a NOTCH-2–DELTA-3 interaction might regulate *slit-1* expression. Similarly, *miR-124* KD led to increased levels of *notch-2* expression and ectopic expression of *slit-1* in the anterior region of the planarians (Fig. S8C, Fig. S6D). These results were further supported by colocalization studies using FISH, which revealed co-expression of *notch-2* and *miR-124* in the periphery of the brain. Together, these results suggest a role for *miR-124* in modulating *notch-2* expression, which is required for regulating *slit-1* in the midline of the anterior regenerating tissue. However, it is still not clear how *miR-124* expression in the brain regulates the *notch-2* domain crucial for *slit-1* expression. Recent studies have shown that miRNAs can be secreted from cells after packaging into exosomes, allowing delivery to adjacent cells and target suppression (Lee et al., 2017). The possibility of an exosome-mediated mechanism to deliver *miR-124* to the *slit-1*⁺ cells needs to be investigated further. Nonetheless, based on our results, we propose a mechanism by which *miR-124* regulates *slit-1* expression via modulation of canonical Notch signaling (Fig. 8B).

The target prediction data from *miR-124* KD animals also revealed the PCP genes *dishevelled-2* and *daam-1* as potential targets of *miR-124*. In planarians, *vang-1*, *daam-1* and *ROCK* KD results in supernumerary eye formation and hyperplasia of neurons throughout the body (Beane et al., 2012). Our results suggest that *miR-124* KD

animals behave like gain-of-function mutants of the PCP pathway, with premature termination of neural growth that leads to a significant decrease in the size of the cephalic ganglia and eyes. However, a rigorous target validation and dissection of the PCP pathway in planarians is necessary to establish whether the *miR-124* family plays a role in regulating this important developmental pathway.

In summary, we report on the development of a novel vehicle to deliver exogenous nucleic acids into planarian cells consisting of co-liposomes designed to have high fusogenic properties with planarian cell membranes. By combining these liposomes with anti-miRs, we were able to robustly target and knock down the function of *miR-124*, resulting in cephalic regeneration phenotypes. Our study reveals the key role of *miR-124* in neuronal organization and axon guidance during regeneration of the brain and visual system in planarians. Such a role for *miR-124* might be found in other neuronal regeneration paradigms.

MATERIALS AND METHODS
Animal maintenance
Schmidtea mediterranea planarians were maintained in 1× Montjuic solution at 20°C. Animals were starved for a week prior to the experiments, as described previously (Sasidharan et al., 2013).

In situ hybridization and immunostaining
Whole-mount *in situ* hybridization (WISH) was performed as previously described (Pearson et al., 2009; Sasidharan et al., 2013; King and Newmark, 2013). miRNA-based WISH was carried out using digoxigenin-labeled miRCURY LNA probes obtained from Exiqon. For immunostaining, animals were fixed using Carnoy's solution as described (Sánchez Alvarado and Newmark, 1999). Rabbit anti-ARRESTIN (1:5000, clone VC-1; gift of Dr Kiyokazu Agata, Kyoto University, Japan) and mouse anti-SYNORF-1 (1:100, DHSB) primary antibodies were used. Species-specific secondary antibodies were obtained from Molecular Probes (1:400). Hoechst 33342 (25 µg/ml; Sigma) was used as a nuclear counterstain. Animals were mounted with Mowiol mounting medium (Sigma) and stored at 4°C until imaging.

Preparation and biophysical characterization of liposomes
Liposomes were prepared with 1:1 molar ratios of lipid and cholesterol at a total concentration of 2 mM. Dry thin films of lipids were prepared in glass vials, followed by overnight hydration with deionized water to produce hydrated films. Vortexing vials for 2-3 min produced multilamellar vesicles. Subsequently, bath sonication (Qsonica sonicator, Q700) produced small unilamellar vesicles. The size and zeta potentials of liposomes (2 mM) were measured using a Zetasizer Nano ZS (Malvern). Using the same method, liposomes with planarian lipids and dual fluorescent lipids (1% of FRET pair, NBD-PE and N-Rho-PE) were made. Fluorescence intensities were recorded by excitation at 485 nm and emission at 530 nm. For the gel retardation assay, Cy3-labeled miRNA (2 µM) was complexed with liposomes in a total volume of 30 µl in HEPES buffer (pH 7.4). The samples were electrophoresed at 80 V for 20 min and the miRNA bands were visualized using an agarose gel documentation unit. Each of the methods used for the biophysical characterization of liposomes is described in more detail in the supplementary Materials and Methods.

Knockdown of *miR-124*, *ovo* and Notch pathway genes
For *miR-124* and *ovo* KD, sexual planarians were pre-pharyngeally amputated, and the head and tail fragments were treated separately with liposome-complexed anti-miRs and scrambled miRs. Notch pathway gene KD was by injecting and feeding dsRNA to intact planarians followed by amputation. Detailed protocols are provided in the supplementary Materials and Methods.

Transcriptome analysis
Total RNA was isolated from scrambled-treated and anti-miR-treated animals (*n*=15) using Trizol (Invitrogen) after two rounds of regeneration. The transcriptome library was prepared from the isolated total RNA using

the TruSeq RNA Library Prep Kit v2 (Illumina) following the manufacturer's instructions. The transcriptome library was subject to paired-end sequencing (150 bp) on a NextSeq 500 next-generation sequencing machine (Illumina). We obtained 54.47 and 91 million reads from *miR-124c* KD and scrambled-treated samples, respectively. We used a reference-based transcriptome assembly algorithm TopHat v2.0.8, Cufflinks v1.0.3 pipeline to assemble the transcripts, with the Ox_Smed_v1 transcriptome as the reference annotation to guide RABT (reference annotation based transcript) assembly. Please refer to the supplementary Materials and Methods for a detailed protocol.

Real-time PCR
Sequencing data were validated by real-time PCR on an ABI PRISM 7900HT. Total RNA used for next-generation sequencing was further used for qPCR validation. Primers are detailed in Table S5. A detailed protocol is provided in the supplementary Materials and Methods.

miRNA target prediction and validation
We used miRanda v3.3a (Enright et al., 2003) to predict targets of *miR-124a*, *b* and *c*. The targets were filtered based on the complementarity score (score ≥140) and free energy (ΔG≤–14 kcal/mol). Target validation was performed in HEK293T cells transfected with pMIR-REPORT plasmid (Addgene) containing the 3′-UTR of the target and pRL-SV40 containing the Renilla luciferase gene (Promega) as a transfection control. miRNA mimics were obtained from Eurogentec and diluted as per manufacturer's instruction. A detailed protocol is provided in the supplementary Materials and Methods.

LNA detection probes, *miR-124* inhibitors and qPCR primers
anti-miR-124 was designed against 16 nucleotides at the 5′ end of *miR-124*. Short probes were used to facilitate better penetrance and substantially reduce cell toxicity, as recommended by the manufacturer. This anti-miR was predicted to KD all *miR-124* family members because these miRNAs share the same seed region and differ by only two or three nucleotides outside the seed region. Please refer to the supplementary Materials and Methods for a detailed list of detection and qPCR probes.

Data availability
RNA-seq data generated in this study have been deposited in the National Center for Biotechnology Information (NCBI) Sequence Read Archive (SRA) database under accession number SRP078739. Original data underlying some of the figures in this manuscript can be accessed from the Stowers Original Data Repository at http://www.stowers.org/research/publications.

Supplementary information
Supplementary information available online at
http://dev.biologists.org/lookup/doi/10.1242/dev.144758.supplemental

References
Adell, T., Cebria, F. and Salo, E. (2010). Gradients in planarian regeneration and homeostasis. *Cold Spring Harb. Perspect. Biol.* **2**, a000505.

Agata, K. and Umesono, Y. (2008). Brain regeneration from pluripotent stem cells in planarian. *Philos. Trans. R. Soc. Lond. B Biol. Sci.* **363**, 2071-2078.

Almuedo-Castillo, M., Salo, E. and Adell, T. (2011). Dishevelled is essential for neural connectivity and planar cell polarity in planarians. *Proc. Natl. Acad. Sci. USA* **108**, 2813-2818.

Beane, W. S., Morokuma, J., Adams, D. S. and Levin, M. (2011). A chemical genetics approach reveals H,K-ATPase-mediated membrane voltage is required for planarian head regeneration. *Chem. Biol.* **18**, 77-89.

Beane, W. S., Tseng, A. S., Morokuma, J., Lemire, J. M. and Levin, M. (2012). Inhibition of planar cell polarity extends neural growth during regeneration, homeostasis, and development. *Stem Cells Dev.* **21**, 2085-2094.

Blassberg, R. A., Felix, D. A., Tejada-Romero, B. and Aboobaker, A. A. (2013). PBX/extradenticle is required to re-establish axial structures and polarity during planarian regeneration. *Development* **140**, 730-739.

Bonar, N. A. and Petersen, C. P. (2017). Integrin suppresses neurogenesis and regulates brain tissue assembly in planarian regeneration. *Development* **144**, 784-794.

Cao, X., Yeo, G., Muotri, A. R., Kuwabara, T. and Gage, F. H. (2006). Noncoding RNAs in the mammalian central nervous system. *Annu. Rev. Neurosci.* **29**, 77-103.

Cao, X. W., Pfaff, S. L. and Gage, F. H. (2007). A functional study of miR-124 in the developing neural tube. *Genes Dev.* **21**, 531-536.

Cebria, F., Kudome, T., Nakazawa, M., Mineta, K., Ikeo, K., Gojobori, T. and Agata, K. (2002a). The expression of neural-specific genes reveals the structural and molecular complexity of the planarian central nervous system. *Mech. Dev.* **116**, 199-204.

Cebria, F., Nakazawa, M., Mineta, K., Ikeo, K., Gojobori, T. and Agata, K. (2002b). Dissecting planarian central nervous system regeneration by the expression of neural-specific genes. *Dev. Growth Differ.* **44**, 135-146.

Cebria, F., Guo, T., Jopek, J. and Newmark, P. A. (2007). Regeneration and maintenance of the planarian midline is regulated by a slit orthologue. *Dev. Biol.* **307**, 394-406.

Chen, J. S., Pedro, M. S. and Zeller, R. W. (2011). miR-124 function during Ciona intestinalis neuronal development includes extensive interaction with the Notch signaling pathway. *Development* **138**, 4943-4953.

Cowles, M. W., Brown, D. D., Nisperos, S. V., Stanley, B. N., Pearson, B. J. and Zayas, R. M. (2013). Genome-wide analysis of the bHLH gene family in planarians identifies factors required for adult neurogenesis and neuronal regeneration. *Development* **140**, 4691-4702.

Currie, K. W., Molinaro, A. M. and Pearson, B. J. (2016). Neuronal sources of hedgehog modulate neurogenesis in the adult planarian brain. *Elife* **5**, e19735.

Enright, A. J., John, B., Gaul, U., Tuschl, T., Sander, C. and Marks, D. S. (2003). MicroRNA targets in Drosophila. *Genome Biol.* **5**, R1.

Fraguas, S., Barberan, S., Iglesias, M., Rodriguez-Esteban, G. and Cebria, F. (2014). egr-4, a target of EGFR signaling, is required for the formation of the brain primordia and head regeneration in planarians. *Development* **141**, 1835-1847.

Friedlander, M. R., Adamidi, C., Han, T., Lebedeva, S., Isenbarger, T. A., Hirst, M., Marra, M., Nusbaum, C., Lee, W. L., Jenkin, J. C. et al. (2009). High-resolution profiling and discovery of planarian small RNAs. *Proc. Natl. Acad. Sci. USA* **106**, 11546-11551.

Fusaoka, E., Inoue, T., Mineta, K., Agata, K. and Takeuchi, K. (2006). Structure and function of primitive immunoglobulin superfamily neural cell adhesion molecules: a lesson from studies on planarian. *Genes Cells* **11**, 541-555.

Gonzalez-Estevez, C., Momose, T., Gehring, W. J. and Salo, E. (2003). Transgenic planarian lines obtained by electroporation using transposon-derived vectors and an eye-specific GFP marker. *Proc. Natl. Acad. Sci. USA* **100**, 14046-14051.

Gonzalez-Estevez, C., Arseni, V., Thambyrajah, R. S., Felix, D. A. and Aboobaker, A. A. (2009). Diverse miRNA spatial expression patterns suggest important roles in homeostasis and regeneration in planarians. *Int. J. Dev. Biol.* **53**, 493-505.

Gurley, K. A., Rink, J. C. and Sánchez Alvarado, A. (2008). Beta-catenin defines head versus tail identity during planarian regeneration and homeostasis. *Science* **319**, 323-327.

Gurley, K. A., Elliott, S. A., Simakov, O., Schmidt, H. A., Holstein, T. W. and Sánchez Alvarado, A. (2010). Expression of secreted Wnt pathway components reveals unexpected complexity of the planarian amputation response. *Dev. Biol.* **347**, 24-39.

Hatfield, S. D., Shcherbata, H. R., Fischer, K. A., Nakahara, K., Carthew, R. W. and Ruohola-Baker, H. (2005). Stem cell division is regulated by the microRNA pathway. *Nature* **435**, 974-978.

Hendrickson, D. G., Hogan, D. J., McCullough, H. L., Myers, J. W., Herschlag, D., Ferrell, J. E. and Brown, P. O. (2009). Concordant regulation of translation and mRNA abundance for hundreds of targets of a human microRNA. *PLoS Biol.* **7**, e1000238.

Higuchi, S., Hayashi, T., Tarui, H., Nishimura, O., Nishimura, K., Shibata, N., Sakamoto, H. and Agata, K. (2008). Expression and functional analysis of musashi-like genes in planarian CNS regeneration. *Mech. Dev.* **125**, 631-645.

Inoue, T., Kumamoto, H., Okamoto, K., Umesono, Y., Sakai, M., Sanchez Alvarado, A. and Agata, K. (2004). Morphological and functional recovery of the planarian photosensing system during head regeneration. *Zoolog. Sci.* **21**, 275-283.

King, R. S. and Newmark, P. A. (2013). In situ hybridization protocol for enhanced detection of gene expression in the planarian Schmidtea mediterranea. *BMC Dev. Biol.* **13**, 8.

Kosik, K. S. (2009). MicroRNAs tell an evo-devo story. *Nat. Rev. Neurosci.* **10**, 754-759.

Lapan, S. W. and Reddien, P. W. (2012). Transcriptome analysis of the planarian eye identifies ovo as a specific regulator of eye regeneration. *Cell Rep.* **2**, 294-307.

Lee, S. T., Im, W., Ban, J. J., Lee, M., Jung, K. H., Lee, S. K., Chu, K. and Kim, M. (2017). Exosome-based delivery of miR-124 in a Huntington's disease model. *J. Mov. Disord.* **10**, 45-52.

Lu, Y. C., Smielewska, M., Palakodeti, D., Lovci, M. T., Aigner, S., Yeo, G. W. and Graveley, B. R. (2009). Deep sequencing identifies new and regulated microRNAs in Schmidtea mediterranea. *RNA* **15**, 1483-1491.

Martin-Duran, J. M., Duocastella, M., Serra, P. and Romero, R. (2008). New method to deliver exogenous material into developing planarian embryos. *J. Exp. Zool. B Mol. Dev. Evol.* **310**, 668-681.

Mootha, V. K., Lindgren, C. M., Eriksson, K. F., Subramanian, A., Sihag, S., Lehar, J., Puigserver, P., Carlsson, E., Ridderstrale, M., Laurila, E. et al. (2003). PGC-1alpha-responsive genes involved in oxidative phosphorylation are coordinately downregulated in human diabetes. *Nat. Genet.* **34**, 267-273.

Mukthavaram, R., Marepally, S., Venkata, M. Y., Vegi, G. N., Sistla, R. and Chaudhuri, A. (2009). Cationic glycolipids with cyclic and open galactose head groups for the selective targeting of genes to mouse liver. *Biomaterials* **30**, 2369-2384.

Ong, T. H., Romanova, E. V., Roberts-Galbraith, R. H., Yang, N., Zimmerman, T. A., Collins, J. J., III, Lee, J. E., Kelleher, N. L., Newmark, P. A. and Sweedler, J. V. (2016). Mass spectrometry imaging and identification of peptides associated with cephalic ganglia regeneration in Schmidtea mediterranea. *J. Biol. Chem.* **291**, 8109-8120.

Orii, H., Mochii, M. and Watanabe, K. (2003). A simple "soaking method" for RNA interference in the planarian Dugesia japonica. *Dev. Genes Evol.* **213**, 138-141.

Palakodeti, D., Smielewska, M. and Graveley, B. R. (2006). MicroRNAs from the planarian Schmidtea mediterranea: a model system for stem cell biology. *RNA* **12**, 1640-1649.

Pearson, B. J., Eisenhoffer, G. T., Gurley, K. A., Rink, J. C., Miller, D. E. and Sánchez Alvarado, A. (2009). Formaldehyde-based whole-mount in situ hybridization method for planarians. *Dev. Dyn.* **238**, 443-450.

Petersen, C. P. and Reddien, P. W. (2009). Wnt signaling and the polarity of the primary body axis. *Cell* **139**, 1056-1068.

Petersen, C. P. and Reddien, P. W. (2011). Polarized notum activation at wounds inhibits Wnt function to promote planarian head regeneration. *Science* **332**, 852-855.

Plasterk, R. H. A. (2006). Micro RNAs in animal development. *Cell* **124**, 877-881.

Rink, J. C., Gurley, K. A., Elliott, S. A. and Sánchez Alvarado, A. (2009). Planarian Hh signaling regulates regeneration polarity and links Hh pathway evolution to cilia. *Science* **326**, 1406-1410.

Roberts-Galbraith, R. H. and Newmark, P. A. (2013). Follistatin antagonizes Activin signaling and acts with Notum to direct planarian head regeneration. *Proc. Natl. Acad. Sci. USA* **110**, 1363-1368.

Roberts-Galbraith, R. H., Brubacher, J. L. and Newmark, P. A. (2016). A functional genomics screen in planarians reveals regulators of whole-brain regeneration. *Elife* **5**, e17002.

Sakai, F., Agata, K., Orii, H. and Watanabe, K. (2000). Organization and regeneration ability of spontaneous supernumerary eyes in planarians -eye regeneration field and pathway selection by optic nerves. *Zoolog. Sci.* **17**, 375-381.

Sánchez Alvarado, A. and Newmark, P. A. (1999). Double-stranded RNA specifically disrupts gene expression during planarian regeneration. *Proc. Natl. Acad. Sci. USA* **96**, 5049-5054.

Sasidharan, V., Lu, Y. C., Bansal, D., Dasari, P., Poduval, D., Seshasayee, A., Resch, A. M., Graveley, B. R. and Palakodeti, D. (2013). Identification of neoblast- and regeneration-specific miRNAs in the planarian Schmidtea mediterranea. *RNA* **19**, 1394-1404.

Seebeck, F., März, M., Meyer, A. W., Reuter, H., Vogg, M. C., Stehling, M., Mildner, K., Zeuschner, D., Rabert, F. and Bartscherer, K. (2017). Integrins are required for tissue organization and restriction of neurogenesis in regenerating planarians. *Development* **144**, 795-807.

Stiles, J. and Jernigan, T. L. (2010). The basics of brain development. *Neuropsychol. Rev.* **20**, 327-348.

Subramanian, A., Tamayo, P., Mootha, V. K., Mukherjee, S., Ebert, B. L., Gillette, M. A., Paulovich, A., Pomeroy, S. L., Golub, T. R., Lander, E. S. and Mesirov, J. P. (2005). Gene set enrichment analysis: a knowledge-based approach for interpreting genome-wide expression profiles. *Proc. Natl. Acad. Sci. USA* **102**, 15545-15550.

Tessier-Lavigne, M. and Goodman, C. S. (1996). The molecular biology of axon guidance. *Science* **274**, 1123-1133.

Thatcher, E. J. and Patton, J. G. (2010). Small RNAs have a big impact on regeneration. *RNA Biol.* **7**, 333-338.

Umesono, Y., Watanabe, K. and Agata, K. (1999). Distinct structural domains in the planarian brain defined by the expression of evolutionarily conserved homeobox genes. *Dev. Genes Evol.* **209**, 31-39.

Vásquez-Doorman, C. and Petersen, C. P. (2014). zic-1 Expression in planarian neoblasts after injury controls anterior pole regeneration. *PLoS Genet.* **10**, e1004452.

Wang, I. E., Lapan, S. W., Scimone, M. L., Clandinin, T. R. and Reddien, P. W. (2016). Hedgehog signaling regulates gene expression in planarian glia. *Elife* **5**, e16996.

Wenemoser, D., Lapan, S. W., Wilkinson, A. W., Bell, G. W. and Reddien, P. W. (2012). A molecular wound response program associated with regeneration initiation in planarians. *Genes Dev.* **26**, 988-1002.

Yamamoto, H. and Agata, K. (2011). Optic chiasm formation in planarian I: Cooperative netrin- and robo-mediated signals are required for the early stage of optic chiasm formation. *Dev. Growth Differ.* **53**, 300-311.

DEVELOPMENT

Biophysical characterization of co-liposomes

1) Zeta Potential (ζ) and Size Measurements:

The sizes and the zeta potentials (surface charges) of the liposomes were measured by photon correlation spectroscopy and electrophoretic mobility on a Zeta sizer NanoZS (Malvern, U.K.). The sizes and potentials of liposomes were measured in deionized water with a sample refractive index of 1.59 and a viscosity of 0.89. The system was validated by using the 200 nmþ5 nm polystyrene polymer (Duke Scientific Corps. Palo Alto, CA). The diameters of liposomes were calculated by using the automatic mode. The zeta potential was measured using the following parameters: viscosity, 0.89 cP; dielectric constant, 79; temperature, 25°C; F(Ka), 1.50 (Smoluchowski); maximum voltage of the current, V. The system was validated by using DTS0050 standard from Malvern, U.K.

2) Fluorescent Resonance Energy Transfer Study:

The membrane fusogenicities were measured for all the liposomes with the same composition used for the transfection studies, i.e., lipid/chol (1:1 mol ratio) as described previously. NBD-PE and N-Rho-PE (Avanti-Polar Lipids, USA) were used as the donor and acceptor fluorescent lipids, respectively. The model planarian biomembrane was prepared using phospholipids isolated from planaria. This model biomembrane formulation was labeled with 0.005 mM NBD-PE and N-Rho-PE lipids (i.e., 1% with respect to the total biomembrane mimicking formulation content). The total lipid concentrations used for all liposomes were the same as that of the biomembrane micking lipid formulation (0.5 mM). Labeled planarian model membrane liposomal formulations were placed in fluorimeter, Microplate Fluoroscence Reader

(Horiba Instruments, USA) at 24°C and equimolar amounts of liposomes with chol/lipid (1:1 mol ratio) were added. Fluorescence intensities were recorded as a function of time with excitation at 485 nm and emission at 530 nm. Fusion (100%) was determined from the NBD-PE fluorescence intensity of the labeled biomembrane liposomal formulation in the presence of 1% Triton X-100.

3) Gel Retardation assay:

MiRNA binding ability of the liposomes were assessed by their gel retardation assay on a 1% agarose gel (pre-stained with ethidium bromide) across the varying Lipid:miRNA charge ratios of 5:1, 10:1 & 20:1. Cy3 labelled miRNA (2 µM) was complexed with the varying amount of cationic liposomes in a total volume of 30 µl in HEPES buffer (pH 7.4) and incubated at room temperature for 20-25 minutes. 5µl of 6x loading buffer (0.25% Bromophenol blue in 40% (w/v) sucrose with sterile H_2O was added to it and from the resulting solution 30µl was loaded on each well. The samples were electrophoresed at 80 V for 20 minutes and the miRNA bands were visualized in the Gel documentation unit.

4) Fluorescence Anisotropy Measurements:

Liposomes were prepared varying the concentration of lipids, symmetric lipid from 0.61mg to 0 mg and asymmetric lipid from 0 mg to 0.63 mg and keeping the co-lipid cholesterol concentration (0.38mg) constant to make final concentration of each individual liposome 1mM. Lipids were dissolved in chloroform along with DPH at a lipid/DPH mole ratio 300:1 and dried under gentle flow of dry nitrogen. The residual solvent was removed under high vacuum for 6-8 h. The dried lipid films were hydrated in 1ml of buffer (Tris-

HCl, pH7.4, 100mM) overnight, vortexed, and sonicated in an ice bath until clarity using a Qsonica sonifier at 100% duty cycle and 5 J output power to produce small unilamellar vesicles (SUVs). The resulting liposomes solutions were used for anisotropy experiments. Anisotropy of DPH was measured by recording the DPH fluorescence values (excitation at 350nm and emission at 420nm) in Horiba fluorescence spectrophotometer.

5) Cy3 labelled oligonucleotides delivery:

Co-liposomes were complexed with cy3 labelled oligonucleotides (IDT) at 2:1 lipid:Cy3 oligo charge ratio in planaria medium (total volume made up to 300 µL) for 15-20 min and treated to the animals. After 48 hrs, animals were treated with N-Acetyl cysteine (NAC) to remove the mucus layer of the animals followed by fixation(4% Formaldehyde) and viewed under a microscope for Cy-3 signals.

Knockdown of *miR-124* and Notch pathway genes

For *miR-124* KD, sexual planarians were pre-pharyngeally amputated, and the head and tail fragments were immediately separated into two different wells in a 24-well plate (nunc). Co-liposome was complexed with *anti-miR-124* and the scramble (10, 50, 100 µM/well) at a 2:1 lipid:*anti-miR* charge ratio in planarian medium (total volume: 300 µL) for 15-20 min and treated for 1 day (until the regenerates were 1 dpa). The animals were treated with the lipoplexes once every 48 h for 7 days. The same set of experiments was repeated for another round to achieve complete knockdown.

RNAi for all Notch pathway genes was performed in asexual planarians using *C. elegans unc-22* as a control. All amputations were made pre- and post-pharyngeally within 2-3 d after last dsRNA treatment unless otherwise indicated. In 7B' and 7C', *in vitro* synthesized dsRNA (Rouhana et al, 2013) was injected 10 times over the course of 41 d using a Nanoject injector (Drummond Scientific, Broomall, PA, USA), and amputations were performed 4 d after last injection. For all other Notch pathway KDs, animals were fed dsRNA synthesized in *E. coli* mixed into a liver paste with 3-4 d between feedings (Gurley et al, 2008). In 7B'' and 7C'', animals were fed dsRNA 6 times. In 7D, animals were fed dsRNA 6 times, amputated, allowed to regenerate for 2 weeks, fed 7 more times, and fixed 1 week after final feeding. In 7F, animals were fed 6 times. Uninjured d*elta-3(RNAi)* animals fed 8 times and imaged 7 d after the final feeding. Regenerating *delta-3(RNAi)* animals were fed 12 times, amputated, and imaged at 16 dpa.

Ovo KD using co-liposomes:

For *ovo* KD, co-liposome was complexed with *ovo* dsRNA at a 2:1 lipid:dsRNA charge ratio in planarian medium (500μl) at room temperature incubated for 30 minutes. The animals was treated with the lipoplexes once in 2 days for 5 days and amputated pre-pharyngeally on the 6th day. 7 dpa animals were scored for phenotypes.

Imaging:

All live animals and WISH staining were imaged on Olympus SX-16 Stereo microscope and Leica M205 Stereo microscope. Fluorescent Whole mount *in*

situ animals and Immuno stained animals were mounted with mowiol and imaged using ZEISS LSM 510 & 780 confocal microscopes. The images were analyzed using Fiji imaging software.

Transcriptome Analysis:

Total RNA was isolated from scramble and anti-miR treated animals by using trizol[tm](Invitrogen) after two rounds of regeneration. Transcriptome library was prepared using the isolated total RNA by using TruSeq RNA Library Prep Kit v2 - Illumina following manufacture's instructions. Transcriptome library was sequenced by performing a paired end sequencing 1*150 on Nextseq-500 NGS machine (illumina). We obtained 54.47, 91 million reads from miR124c-KO & scrambled samples. We used reference based transcriptome assembly algorithms Tophat v2.0.8, Cufflinks v1.0.3 pipeline to assemble the transcripts with Ox_Smed_v1 [67] transcriptome as reference annotation to guide RABT assembly. Older version of cuffdiff v1.0.3 gives better results compared to newer version when samples lack biological replicate. So we used an older version of cuffdiff v1.0.3 to identify differentially expressed genes. In the absence of the biological replicates, Cuffdiff applied a Poisson distribution to account for technical variation in the data. The variance was measured across the conditions under the assumption that most transcripts were not differentially expressed. Based on this assumption, P-values were derived for all genes. We considered that transcripts that have adjusted pvalue < 0.05 to be significantly expressed (Supplemental table). We identified 2227 transcripts as significantly expressed. We used Trinotate v-2.0.2 (*http://trinotate.github.io*) to annotate Ox_Smed_v1 transcriptome. We

performed GO analysis for up & down regulated transcripts using hmmer2go tool (https://github.com/alexharkess/HMMER2GO) and the GO terms were clustered using REVIGO (Supek et al., 2011). To analyze the pathways that were enriched in knock down we used GSEA(Subramanian et al., 2005, Mootha et al., 2003). Background database used for this search is BIOCARTA, KEGG, REACTOME, and CANONICAL PATHWAYS. Cut-off used for filtering is top 100 pathways with FDR qvalue < 0.05 (Supplemental table). The data generated in the study has been deposited in the National Center for Biotechnology Information (NCBI), Sequence Read Archive (SRA) database. Accession ID: SRP078739.

Details of LNA detection probes, miR-124 inhibitors and q-PCR primers:

The *anti-miR* was designed against 16 nucleotides at the 5' end of *miR-124*. Short probes were used to facilitate better penetrance substantially reduce cell toxicity, as recommended by the manufacturer. This *anti-miR* was predicted to KD all *miR-124* family members because these microRNAs share the same seed region and they differ by only 2-3 nucleotides outside the seed region. LNA detection probes and inhibitors were procured from Exiqon,Denmark. Please find the probe details below

Detection Probe	Product no	Batch no
Sme-miR-124c 3P(dig)	32005-15	140791
Sme-miR-124a 3P(dig)	80040-15	140627
Sme-miR-124b 3P(dig)	80041-15	140628
Sme-miR-124e 3P(dig)	699998-341	620084
Sme-miR-124c 3P(Fam)	99999-04	182954

Inhibitor Probes	Product no	Batch no
i-sme-mir-scr	199900	161265
i-sme-mir-124	199900	161264
Q-PCR primers	Product no	Batch no
Sme-miR-124a 3p	2100183	620664
Sme-miR-124b 3p	2100802	620655
Sme-miR-124c 3p	2111945	620666

Real time PCR:

Sequencing data was validated using Real time PCR (Abiprism 7900HT ABI). Total RNA used for NGS was further used for q-PCR validation. First strand synthesis was done using Superscript II Reverse transcriptase (Invitrogen) according to manufacture's protocol. Candidate gene expression was calculated using ct values using delta delta ct method keeping actin as control (Jozefczuk and Adjaye, 2011). Primer details are given in Table S5.

miRNA target prediction and validation:

We used miRanda v3.3a (Enright et al., 2003) to predict targets of miR124c-3p. miRanda predicts target of miRNA based on seed region complementarity with mRNA and checks whether the binding is thermodynamically favorable. The targets were filtered based on the complementarity score (score ≥140) calculated from algorithm as well as free energy of optimal strand-to-strand interaction between mRNA and miRNA sequence ($\Delta G \leq -14$Kcal/mol). Primers were designed to clone the 3'UTR regions of the target genes and cloned into the 3'UTR region of Firefly

luciferase in pMIR REPORT plasmid (addgene). HEK 393T cells were transfected with pMIR REPORT plasmid containing the 3'UTR of target and pRL-SV40 containing renilla luciferase gene (promega) as transfection control. MiRNA mimics was procured from eurogentec and diluted as per manufacture's instruction. Both the constructs were co transfected with 25nM and 50nM concentration of miRNA mimics. After 36 hours post transfection cell were lysed (Dual Glo promega luciferase kit) and relative luciferase expression was measured using berthold Sirius luminometer.

Figure S1

A

B

C

D
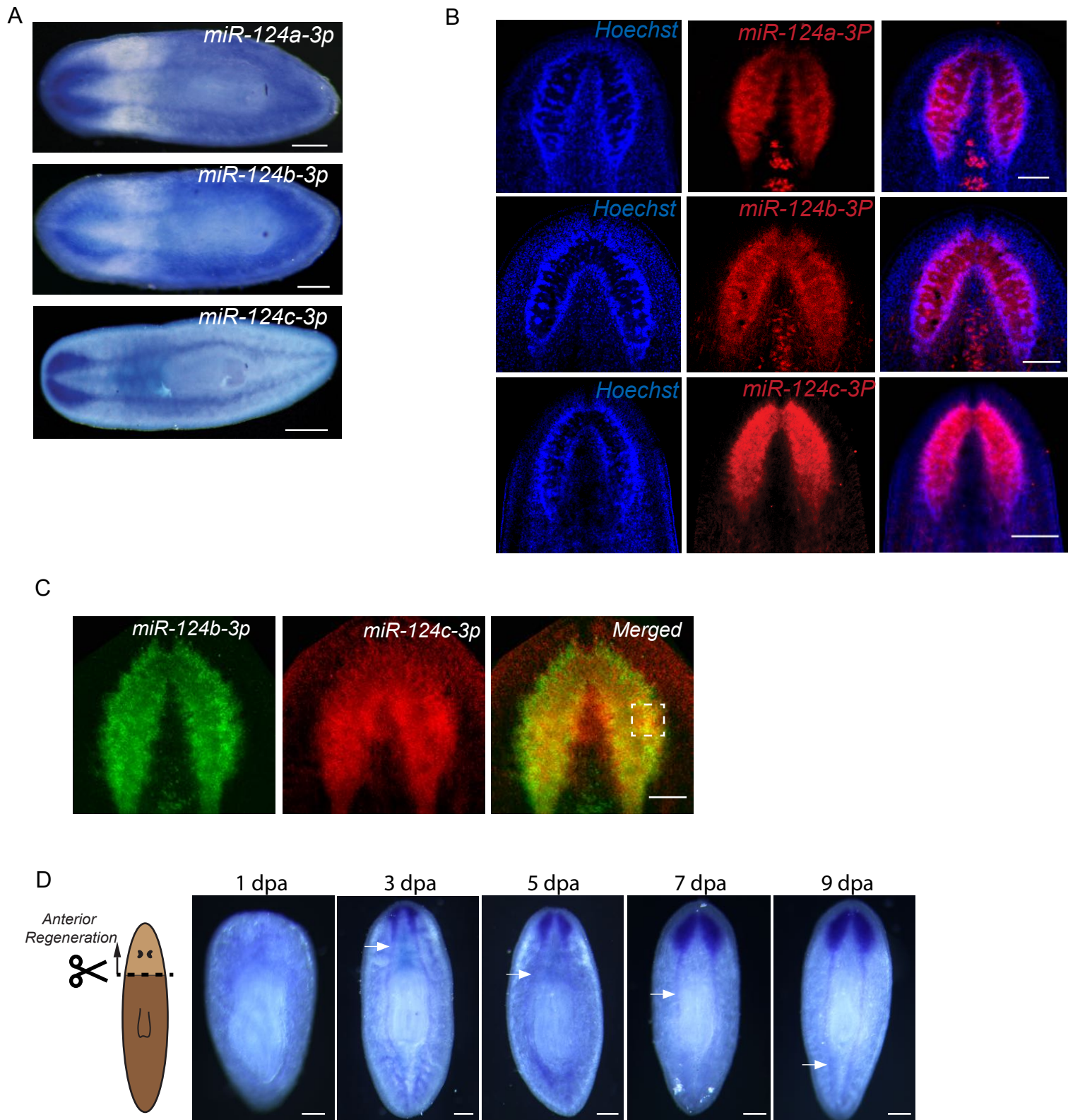
Fig. S1. A) Colorimetric WISH for *miR-124a, b*, and *c* on uninjured planarians. Representative images of n=5 animals each. B) *FISH* for *miR-124a, b*, and *c* (red) with nuclear counterstain (Hoechst 33342, blue) shows that *miR-124c* displays a broader expression domain in the brain compared to *miR-124a* or *-b*. C) Double *FISH* for *miR-124b* (dig probe,green) and *miR-124c* (fam probe,red). Dashed box in the inset of merged figure represents the area shown in Fig.2B. Representative image of n=5 animals. D) Colorimetric *WISH* for *miR-124c* on animals regenerating heads at indicated timepoints. White arrow indicates the posterior extent of *miR-124c* expression in the pre-existing ventral nerve cords. Representative images from n=4 animals each. All scale bars in A-D are 100 μm.
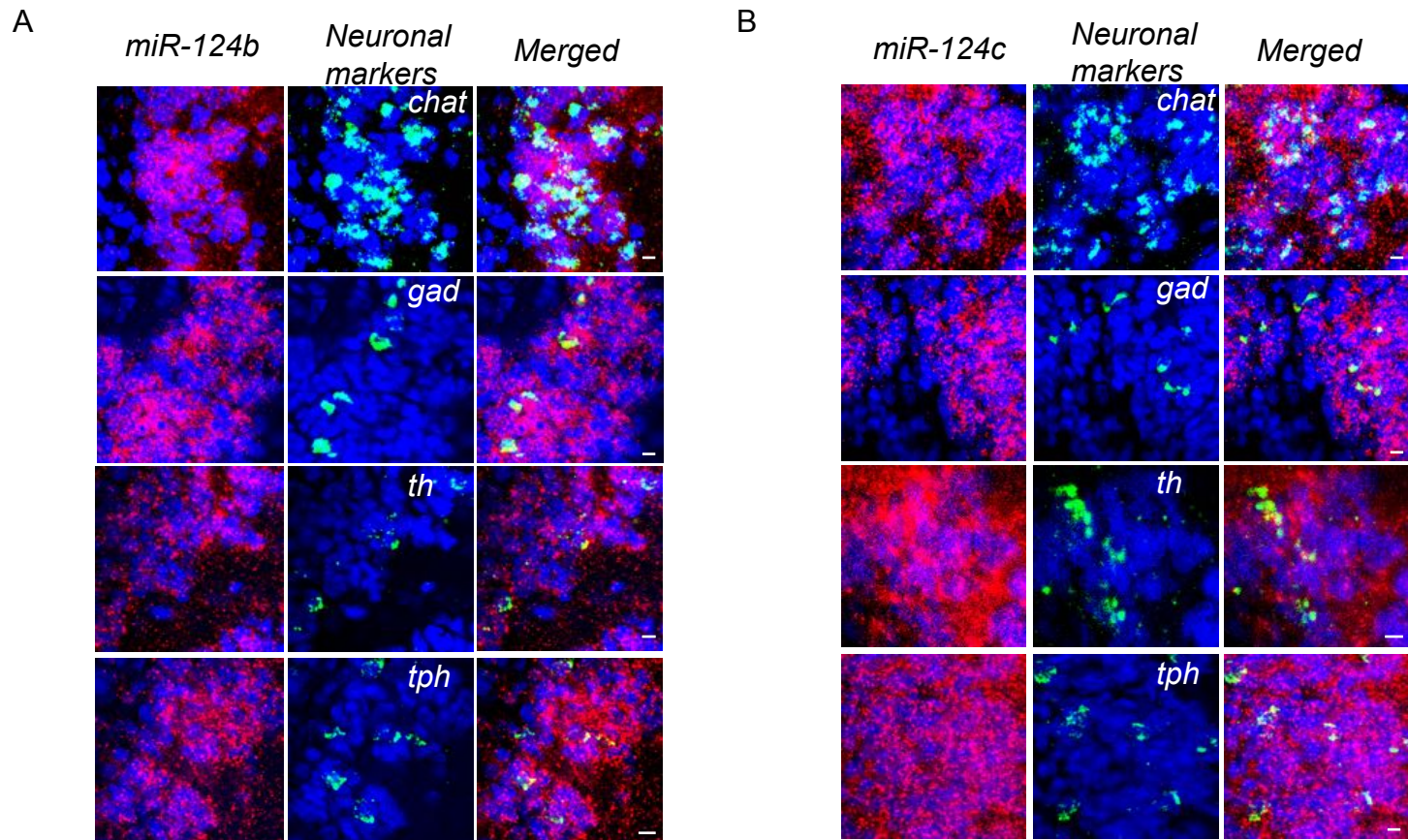
Figure S2

Figure S2. Co-expression of neural subtype markers with miR-124 family miRNAs. A&B) Double FISH was performed using different neural subtype markers labeling cholinergic, GABAergic, dopaminer-gic, and serotonergic neurons (green) and miR-124 family miRNAs(miR-124b and C, red), Counterstained with nuclear dye (Hoechst 33342, blue). These high magnification images were obtained from 3-5 microns optical section, showing co expression of the neural subtype markers with the miR-124 family miRNAs in the same cells. Scale bar represents 12μm.

Figure S3
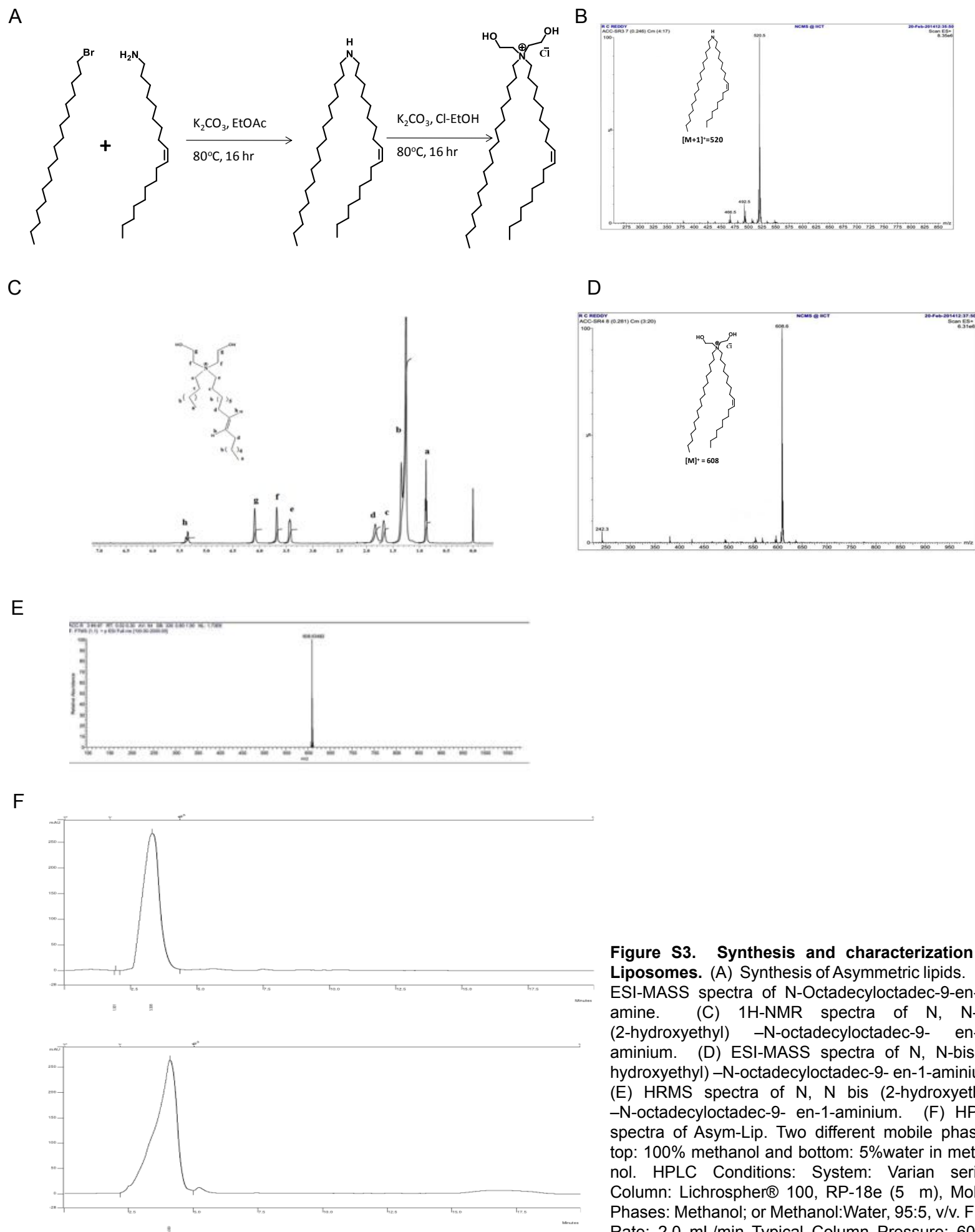
Figure S3. **Synthesis and characterization of Liposomes.** (A) Synthesis of Asymmetric lipids. (B) ESI-MASS spectra of N-Octadecyloctadec-9-en-1-amine. (C) 1H-NMR spectra of N, N-bis (2-hydroxyethyl) –N-octadecyloctadec-9- en-1-aminium. (D) ESI-MASS spectra of N, N-bis (2 hydroxyethyl) –N-octadecyloctadec-9- en-1-aminium. (E) HRMS spectra of N, N bis (2-hydroxyethyl) –N-octadecyloctadec-9- en-1-aminium. (F) HPLC spectra of Asym-Lip. Two different mobile phases; top: 100% methanol and bottom: 5%water in metha-nol. HPLC Conditions: System: Varian series, Column: Lichrospher® 100, RP-18e (5 m), Mobile Phases: Methanol; or Methanol:Water, 95:5, v/v. Flow Rate: 2.0 mL/min Typical Column Pressure: 60-65 Bars, Detection: UV at 210 nm.

Figure S4

A
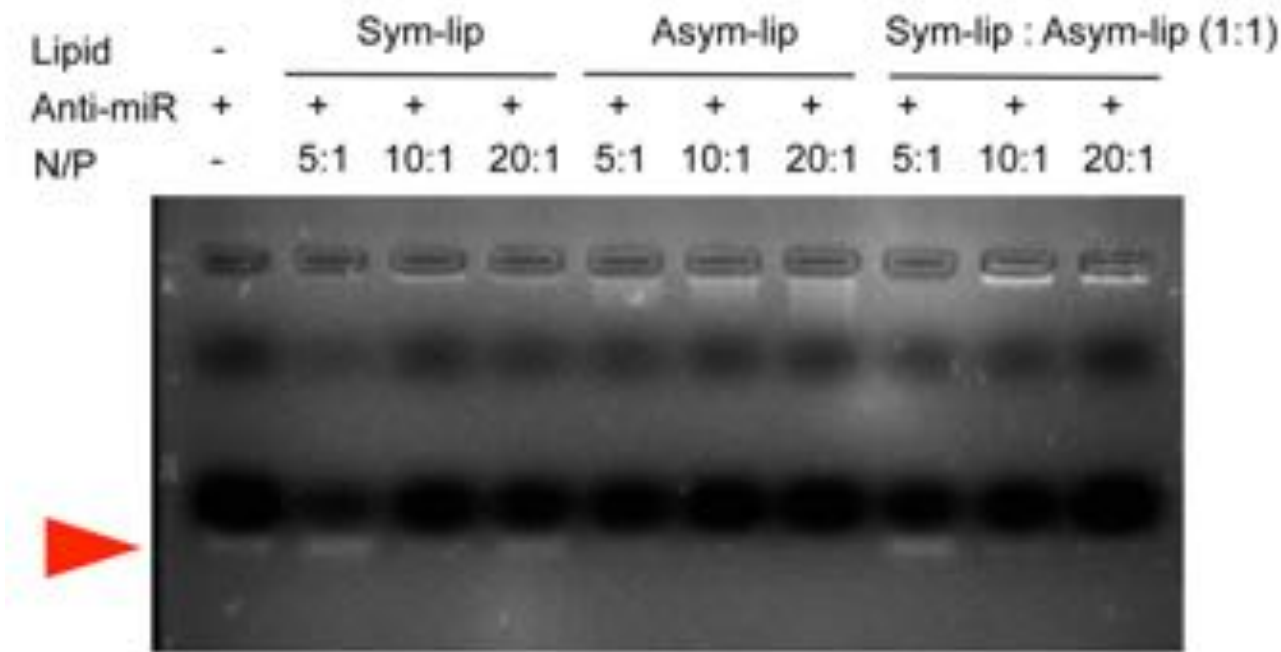
B
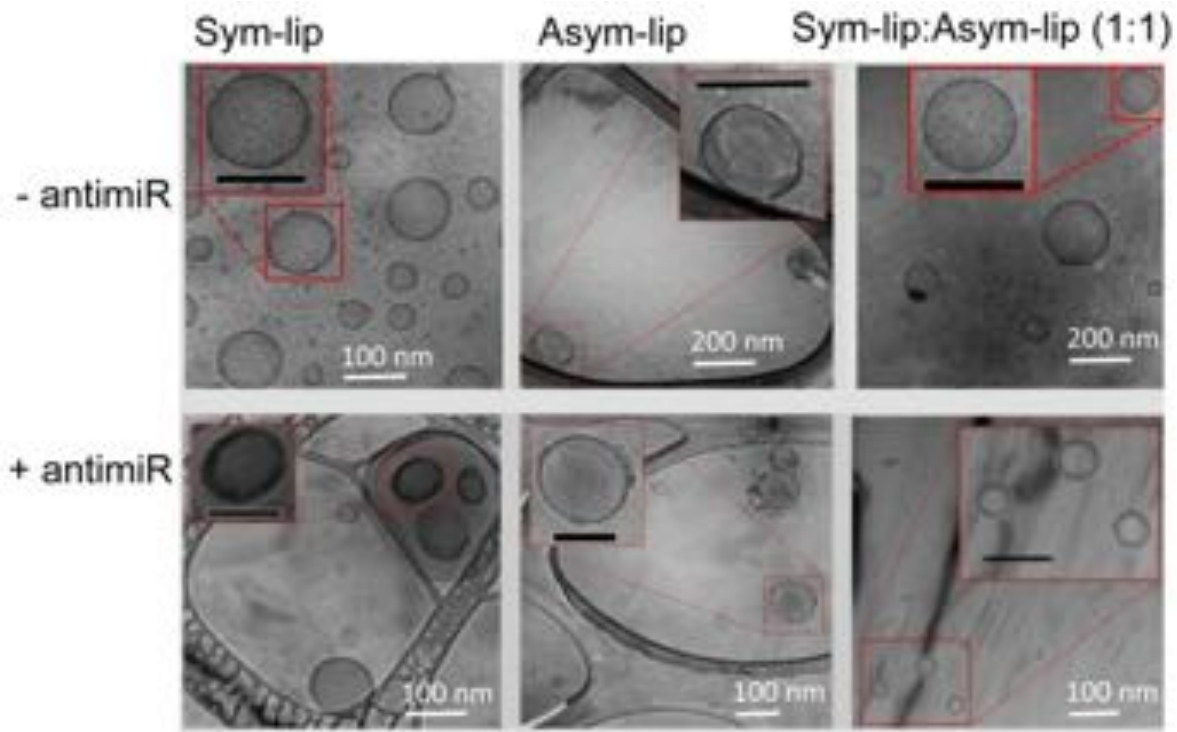
Fig S4. Characterization of Liposomes. (A) Gel retardation assay for complexes of liposomes and anti-miRs. Red arrow head shows the non-stabilized nucleic acid. (B) Scanning electron microscope images of liposomes and lipoplexes prepared from Asym-Lip and Sym-Lip and combination of both lipids.
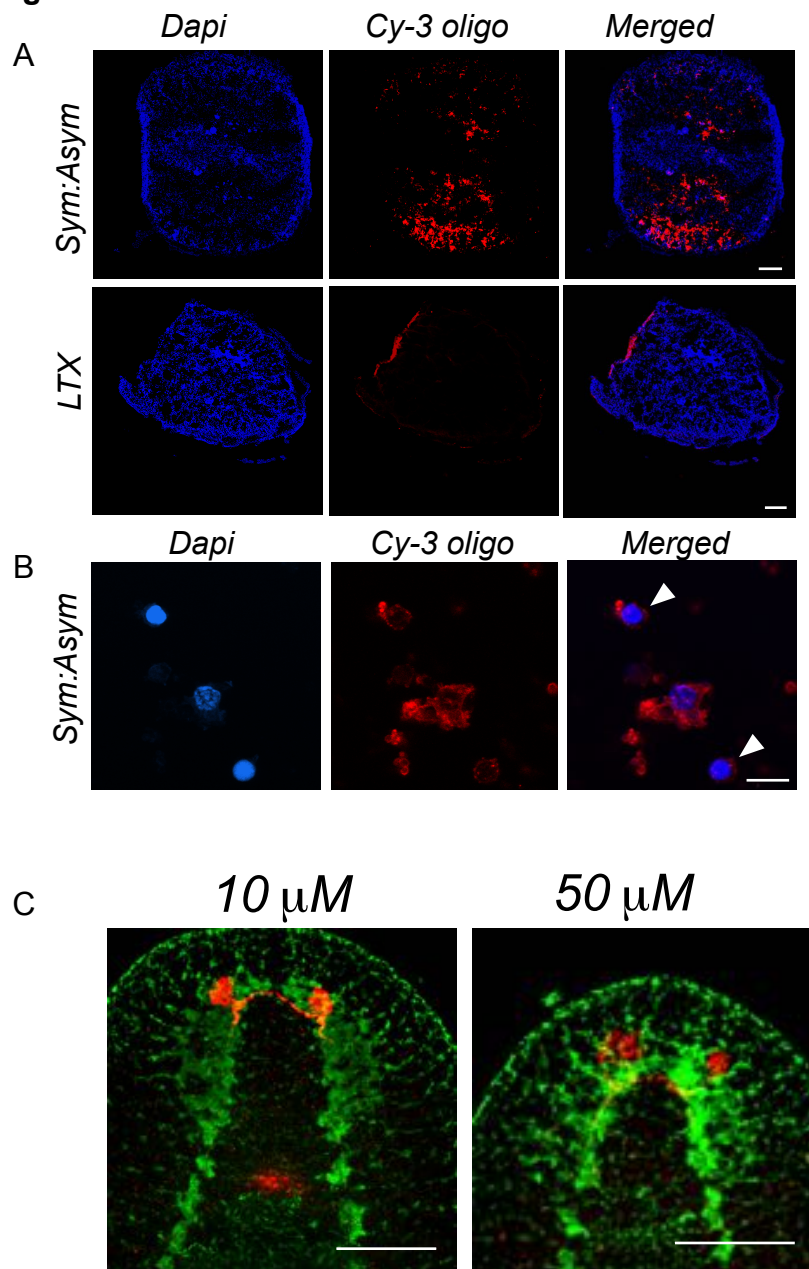
Figure S5

Fig. S5. Delivery of cy-3 oligos into planarian tissues using co-liposomes and characterization of *miR-124-KD*. A) 1 dpa animals devoid of head and tail fragments were transfected with cy-3 labeled oligos using co-liposomes (Sym:Asym) or commercially available Lipofectamine (LTX). After 2 days of transfection, animals were treated with 5% n-acetyl-cysteine, followed by 4% formaldehyde fixation. Tissues were cryosectioned (16 µm-thick) and nuclear counterstained (DAPI, blue). Cy-3 oligos (red) penetrated planarian tissues more effectively when transfected using novel liposomes when compared to using LTX. Representative images of n=4 animals each. Scale bar, 100 µm. B) Transfected animals were macerated into single-cell suspensions and post-fixed using 4% formaldehyde before confocal imaging. White arrowheads indicate cells successfully transfected with Cy-3 oligos (red). Nuclei counterstained with Hoechst (blue). Scale bar, 10 µm. C) The visual neurons (anti-ARRESTIN, red) and brain (anti-SYNORF-1, green) are indistinguishable between animals treated with 10 and 50 µM *anti-miR-124* in 7 dpa following 2 rounds of regeneration. Representative images of n=10 animals. Scale bar 100 µm.
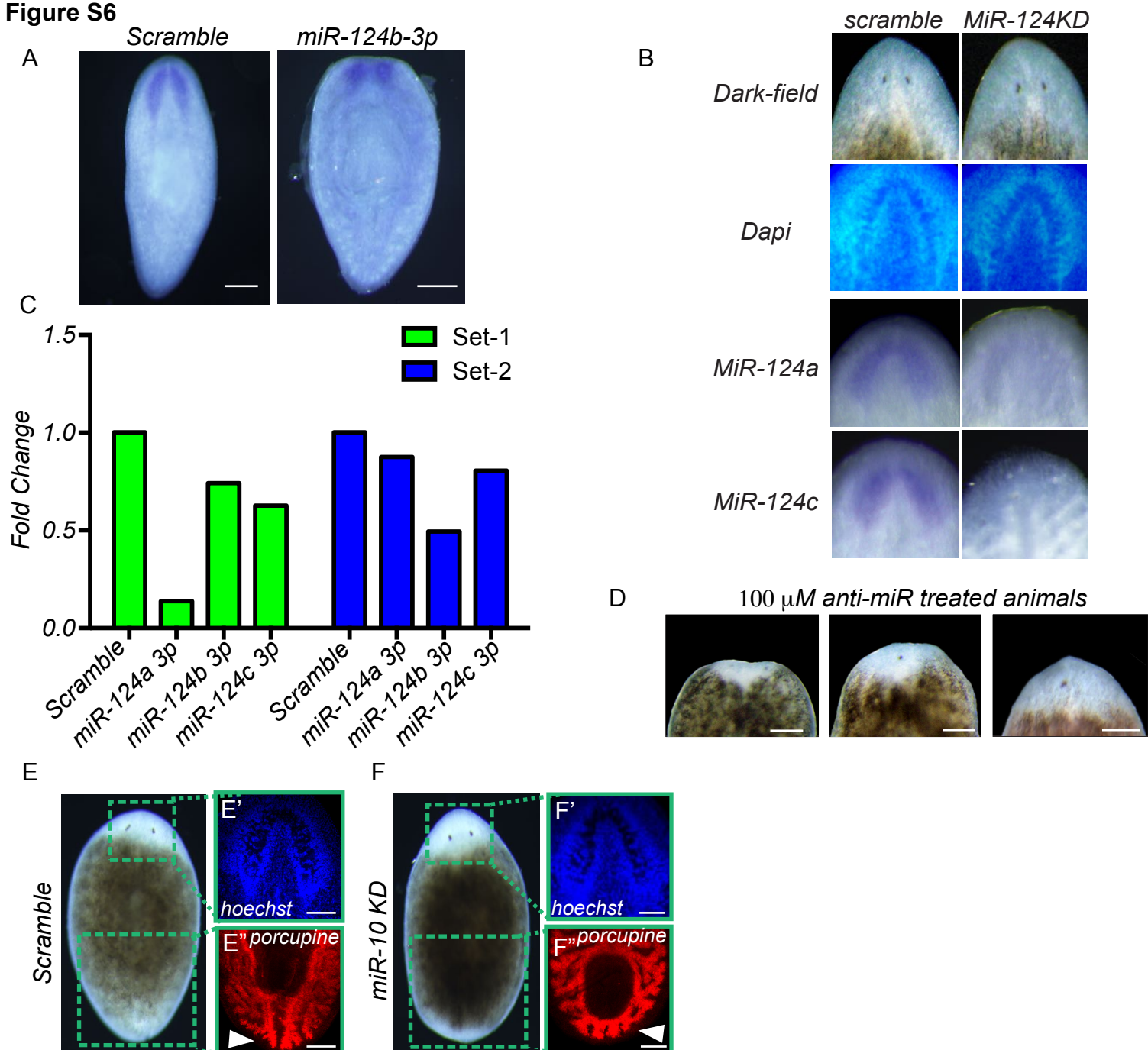
Figure S6

Fig. S6. Delivery of miRNA inhibitors using liposomes yields robust and specific regeneration defects. A) Colorimetric *WISH* for *miR-124b* following treatment with 100 µM *anti-miR-124* . Compared to scrambled-treated controls, animals regenerating head tissue showed significant loss of *miR-124b* expression at 7 dpa of the second round of regeneration. Scale bar, 100 µm. B) Live images of animals after 1st round of ant-miR treatment. There were no phenotypes observed after 1st round of regeneration (15/15). *MiR-124* anti-miR treated animals were stained with dapi to visualize the brain organization.   Colorimetric *WISH* for *miR-124a and c* following treatment with 100 µM *anti-miR-124* after first round of regeneration was performed. C) Fold-change in expression levels of *miR-124* family miRNAs (*miR-124a, -b, and -c*) compared to the scrambled-treated controls. Fold-change was determined by q-PCR using specific LNA probes (Exiqon) on 100 µM *anti-miR-124* KD animals. Two biological replicates (set 1, green; set 2, blue) were performed. D) Live images of animals treated with 100 µM *anti-miR-124* showing representative eye regeneration deformities. Scale bar, 100 µm. E-F) To assess specificity of miRNA knockdown using liposomes, the *miR-10* family was knocked down and animals were amputated pre- and post-pharyngeally at 7 dpa following two rounds of regeneration. Knockdown of *miR-10* does not disrupt regeneration of the eyes (live images) or brain (Hoescht [nuclei], blue), but it does cause fusion of the posterior gut branches (porcupine-1, red) in 7/10 animals. Scale bar, 100 µm.

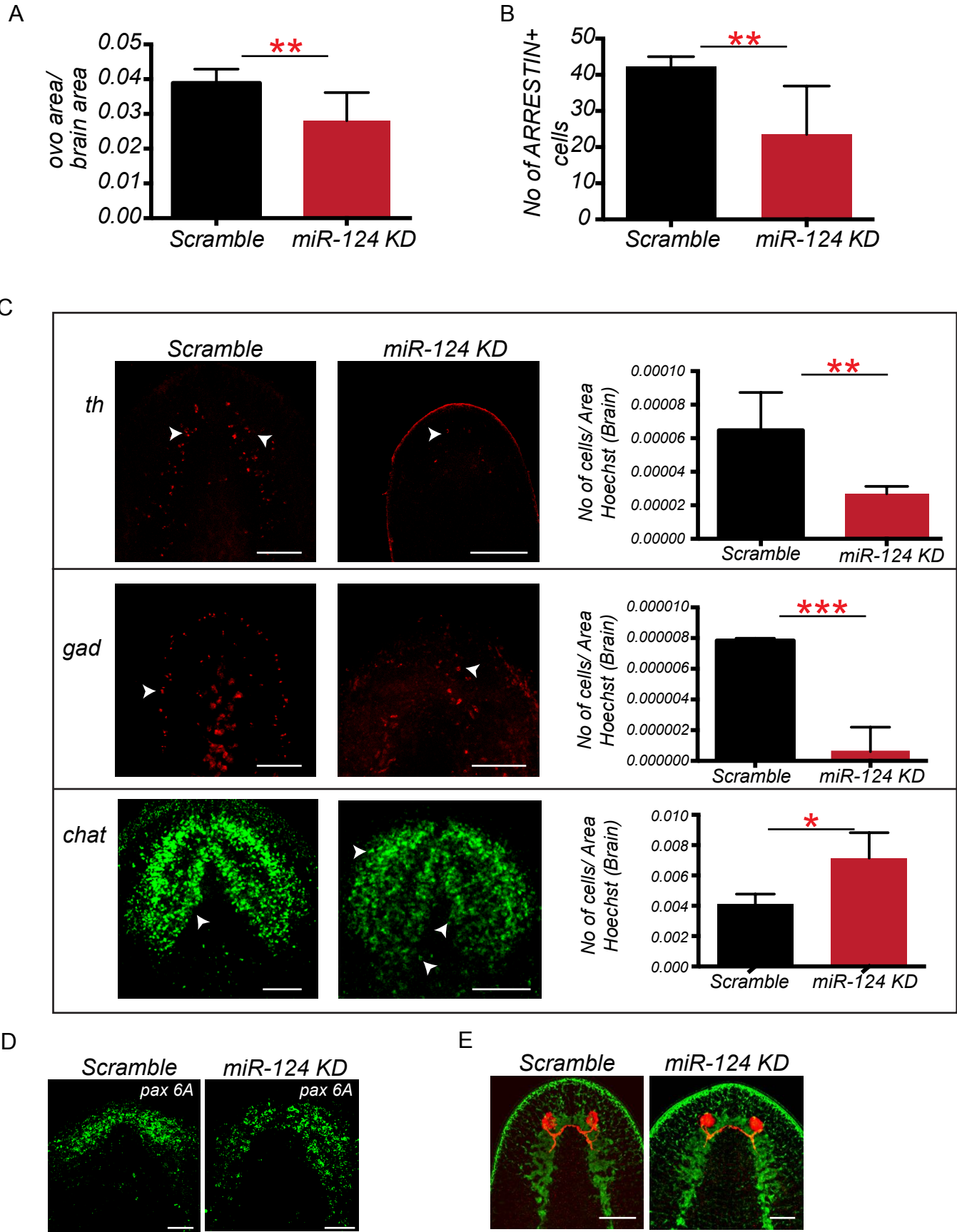**Figure S7**

A

B

C

D

E

Fig. S7. Knockdown of *miR-124* perturbs regeneration of discrete neural populations in brain and visual system. A) Quantification of the size of regenerated eyes (area of ovo staining) normalized to brain area in scrambled (n=5) versus *anti-miR-124*-treated (n=6) planarians in 7 dpa animals following 2 rounds of regeneration. KD of *miR-124* significantly reduces the size of the regenerated eyes. B) Quantification of the numbers of regenerated PRNs (anti-ARRESTIN+ cells) in similarly sized scrambled- versus anti-*miR-124* treated planarians in 7 dpa animals following 2 rounds of regeneration. KD of *miR-124* results in a two-fold reduction in numbers of PRNs. C) *FISH* for three neuronal subtypes in scrambled- versus *anti-miR-124* treated planarians, and quantifications of each population normalized to brain area in 7 dpa animals following 2 rounds of regeneration. Loss of *miR-124* caused a significant reduction in the numbers of *th*+ neurons (n=5/5 animals) and *gad*+ neurons (n=5/5 animals), in addition to an increase in numbers of *chat*+ neurons (n=6/6 animals). D) FISH for neural progenitors (*pax6A*, green) in scrambled- versus *anti-miR-124* treated planarians (100 mM anti-miRs) antimiR treated animals in regenerated head tissue at 4 dpa following 2 rounds of regeneration. *Pax6A* expression is not affected by KD of *miR-124* (n=6/6 animals). E) Uninjured animals treated with scrambled- or *anti-miR-124* (100 µM) for 1 month. The visual neurons (anti-ARRESTIN, red) and brain (anti-SYNORF-1, green) were unaffected during homeostasis. Representative images of n=10 animals each. Scale bars in C-E represent 100 µm. *P < 0.05, **P < 0.01, ***P < 0.001 (Student's t-test).
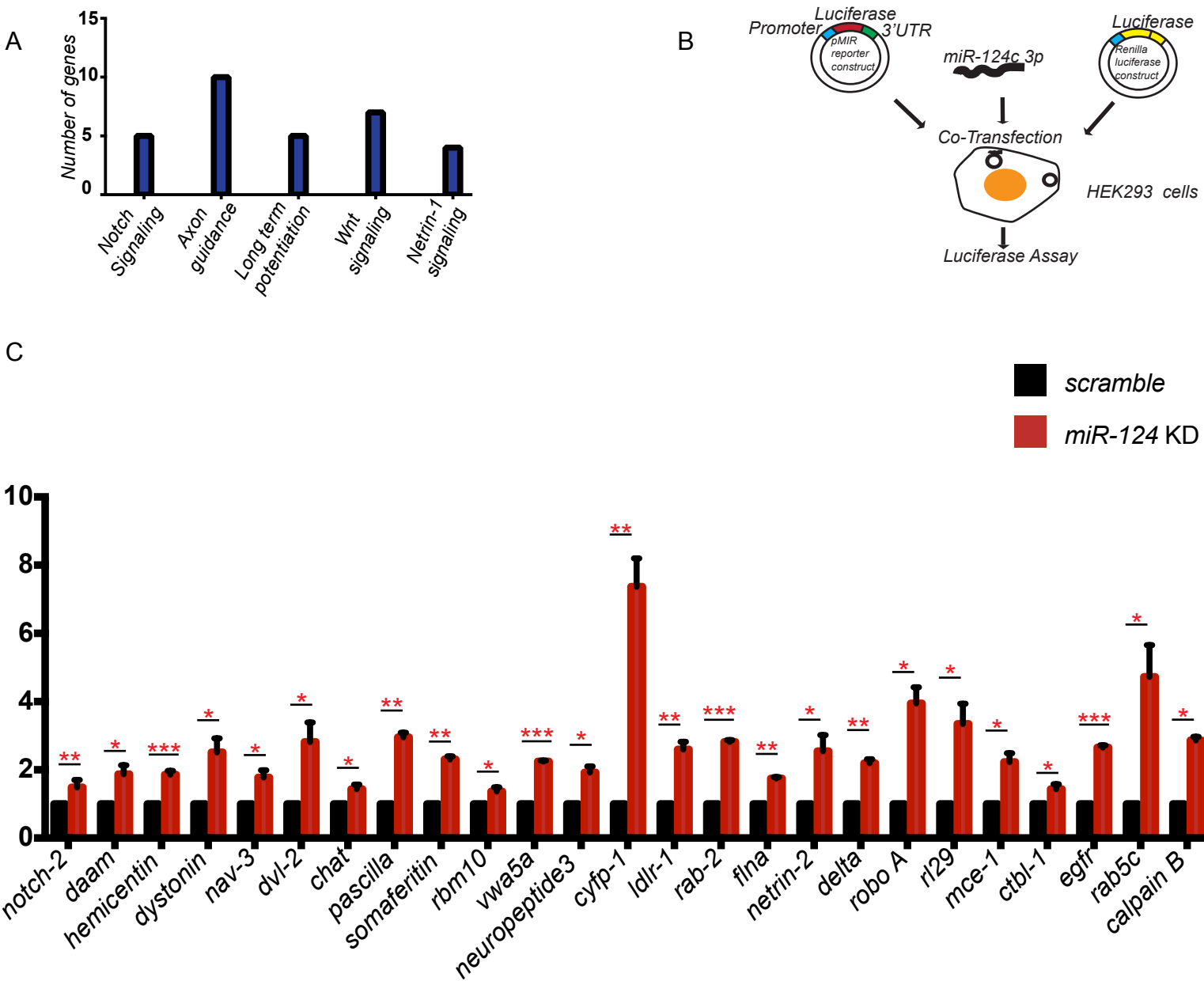
Figure S8

Fig. S8. Pathway analysis and biological function of miR-124 targets. (A) Bar graph shows the Gene Set Enrichment Analysis of miR-124 targets predicted by miRANDA. (B) Pictorial description of target prediction using luciferase assay system in a heterologus system. (C) Q-PCR validation of upregulated targets upon *miR-124 KD*. *P < 0.05, **P < 0.01, ***P < 0.001 (Student's t-test).
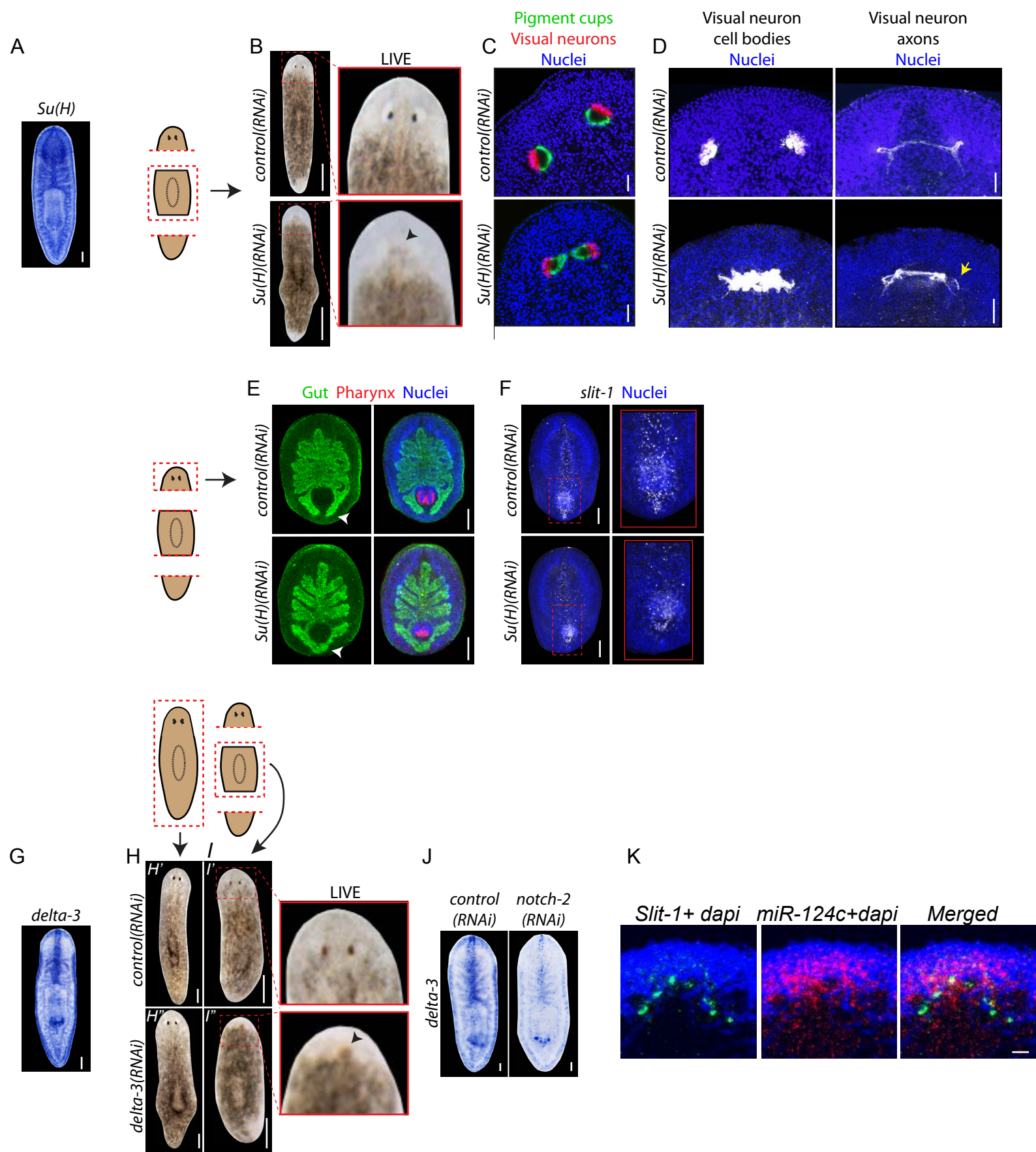
Figure S9

Fig. S9. Canonical Notch signaling maintains midline polarity in planarians. (A) *WISH* on uninjured asexual planarian for the Notch pathway transcription factor, *Su(H)*. (B) Live control- and *Su(H)(RNAi)* planarians. A mid-body bulge and cyclopia are observed after knockdown of *Su(H)*, similar to *notch-2(RNAi)* animals. 14 dpa trunk regenerates following 10 dsRNA injections. Scale bars, 250 μm. (C) Eyes of control- versus *Su(H)(RNAi)* planarians. *FISH* for pigment cup cells (*tyrosinase*, green), photosensing neurons (*opsin*, red), and nuclei (DAPI, blue) shows cyclopia after knockdown of *Su(H)*. 10 dpa trunk regenerates following 3 dsRNA injections. (D) Photosensing neurons and their axon projections in control- versus *Su(H)(RNAi)* planarians. *Su(H)(RNAi)* planarians display fusion of photosensing neurons (cyclopia) and disruption of the optic chiasm, similar to *slit-1*(RNAi) animals (Cebrià et al., 2007). Arrow indicates fasciculation/disorganization of ventral axonal projections. 6 dpa trunk regenerates following 3 dsRNA injections. (E) Morphology of the gastrovascular system in control- versus Su(H)(RNAi) planarians. FISH shows the gut (*mat-1*, green), pharynx (*DNAH-β3*, red), and nuclei (DAPI, blue). Arrowhead highlights posterior gut branch fusion in *Su(H)*(RNAi) planarians. 7 dpa head regenerates following 3 dsRNA injections. (F) *FISH* for midline (*slit-1*, white) and nuclei (DAPI, blue) in control- versus *Su(H)*(RNAi) planarians. *Slit-1+* cells are reduced after RNAi of *Su(H)*. 6 dpa head regenerates following 3 dsRNA injections. (G) Colorimetric *WISH* on uninjured adult asexual planarian for *delta-3*. (H) Uninjured live control(RNAi) (H'.) versus *delta-3*(RNAi) (H") planarians. Delta3(RNAi) planarians display a midbody bulge similar to *notch-2* and *Su(H)*(RNAi) animals. 16 dpa live control(RNAi) (I') versus *delta-3*(RNAi) (I") planarians. *Delta-3*(RNAi) planarians display cyclopia similar to *notch-2* and *Su(H)*(RNAi) animals. (J) Colorimetric *WISH* on control- versus *notch-2*(RNAi) planarians. *Delta-3* expression is reduced after knockdown of *notch-2*. (A-J) All scale bars are 100 μm unless otherwise noted. (K) *Slit-1* and *miR-124c* co expression in 3 dpa animals. These high magnification images were obtained from 3 microns optical section, showing co expression of slit-1 with the *miR-124* family miRNAs in the same cells. Scale bar represents 15μm.
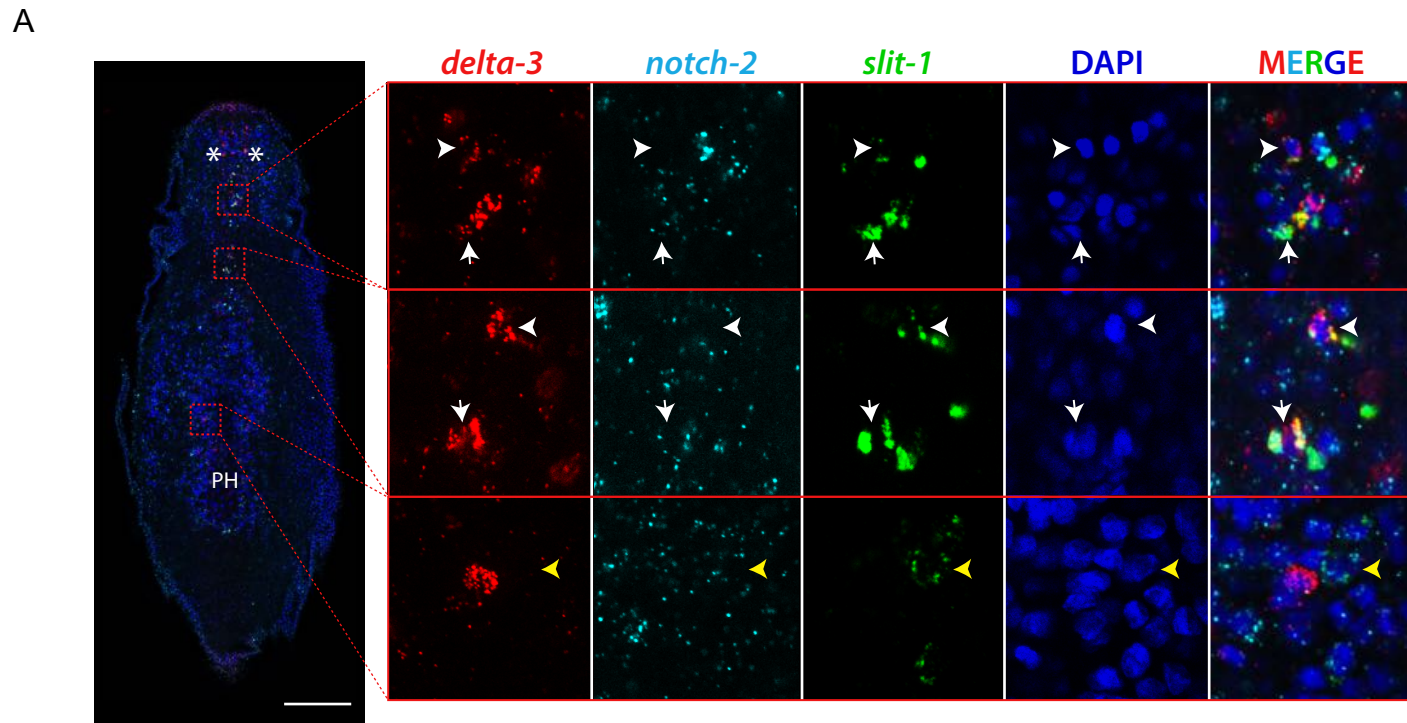
Figure S10

Fig. S10. Colocalization of notch pathway genes and midline marker. A) *FISH* of an uninjured planarian for *delta-3* (red), *notch-2* (cyan), *slit-1* (green, midline marker), and nuclei (DAPI, blue). White arrowheads indicate representative delta-3+/notch-2- midline cells. Yellow arrowheads indicate representative delta-3-/notch-2+ midlinecells. White arrows indicate representative delta-3+/notch-2+ midline cells. Three different single confocal z-slices are shown, captured from the indicated locations in the whole worm. Asterisks, eyes. PH, pharynx. Scale bar, 200 μm.

Figure S11

A

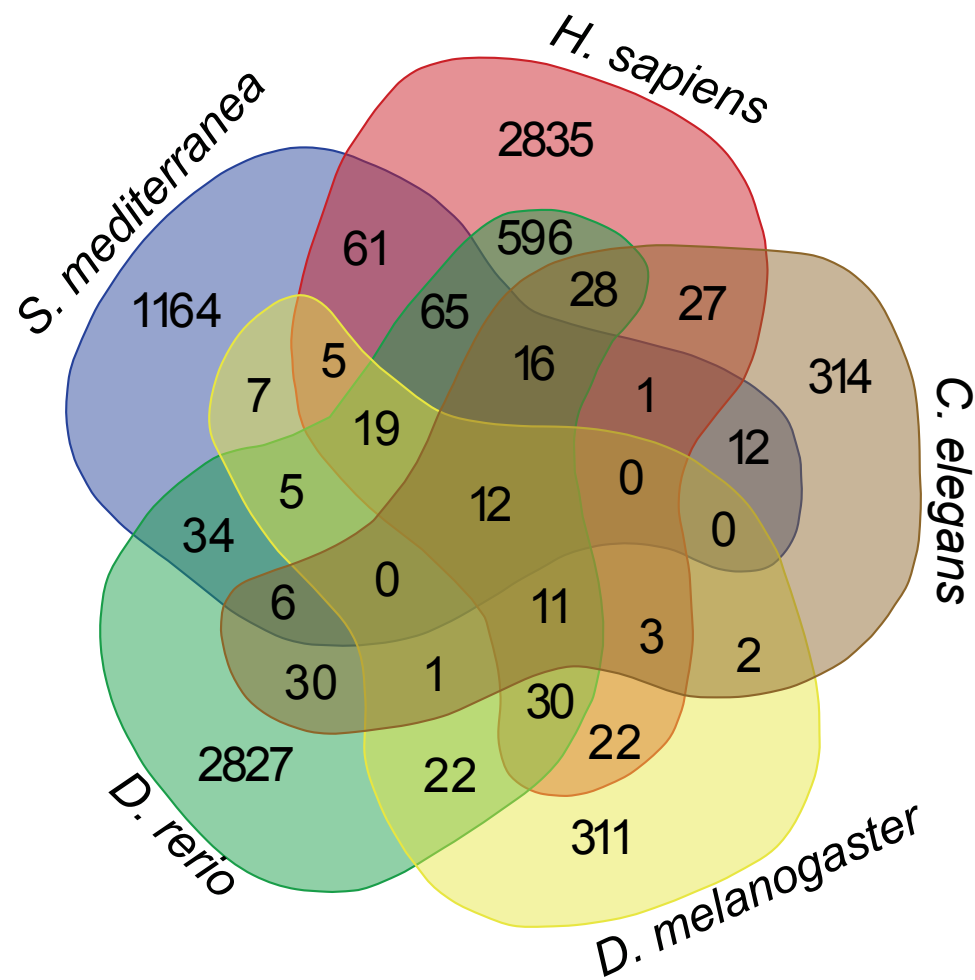Fig. S11. **Conservation of *miR-124* targets across *spp.*.**Venn diagram showing the conservation of *miR-124* targets across *H. sapiens, D. rerio, C. elegans, D. melanogaster, and S. mediterranea.*

Table S1. miR-124 targets

Click here to Download Table S1

Table S2. GSEA of miR-124 targets

Click here to Download Table S2

Table S3. List of upregulated targets upon miR-124 KD

Click here to Download Table S3

Table S4. Conservation of miR-124 targets across spp.

Click here to Download Table S4

Table S5. List of primers

Click here to Download Table S5